

Alaska-Aleutian megathrust:

Variation in subducting plate structure and implications for seismicity offshore Alaska

by

Mitchell Grace

Supervisors: Keith Louden and Mladen Nedimović

Submitted in partial fulfilment of the requirements for the  
degree of Combined Honours Bachelor of Science in Earth Sciences and Oceanography

at

Dalhousie University  
Halifax, Nova Scotia  
April, 2014

© Mitchell Grace, 2014

## Distribution License

DalSpace requires agreement to this non-exclusive distribution license before your item can appear on DalSpace.

### NON-EXCLUSIVE DISTRIBUTION LICENSE

You (the author(s) or copyright owner) grant to Dalhousie University the non-exclusive right to reproduce and distribute your submission worldwide in any medium.

You agree that Dalhousie University may, without changing the content, reformat the submission for the purpose of preservation.

You also agree that Dalhousie University may keep more than one copy of this submission for purposes of security, back-up and preservation.

You agree that the submission is your original work, and that you have the right to grant the rights contained in this license. You also agree that your submission does not, to the best of your knowledge, infringe upon anyone's copyright.

If the submission contains material for which you do not hold copyright, you agree that you have obtained the unrestricted permission of the copyright owner to grant Dalhousie University the rights required by this license, and that such third-party owned material is clearly identified and acknowledged within the text or content of the submission.

If the submission is based upon work that has been sponsored or supported by an agency or organization other than Dalhousie University, you assert that you have fulfilled any right of review or other obligations required by such contract or agreement.

Dalhousie University will clearly identify your name(s) as the author(s) or owner(s) of the submission, and will not make any alteration to the content of the files that you have submitted.

If you have questions regarding this license please contact the repository manager at [dalspace@dal.ca](mailto:dalspace@dal.ca).

Grant the distribution license by signing and dating below.

---

Name of signatory

---

Date

## TABLE OF CONTENTS

Table of contents.....	ii
List of figures .....	iii
Abstract.....	v
List of abbreviations used.....	vi
Acknowledgements.....	vii
Introduction.....	1
Methods.....	3
Data Acquisition .....	3
Processing .....	6
3. Results.....	19
Line 2 .....	19
Line12E.....	21
4. Discussion.....	37
Literature cited .....	43

## LIST OF FIGURES

Figure 1.1.1	Study area map with seismic line locations	2
Figure 2.1.1	Air gun array	4
Figure 2.1.2	Tow array offsets	4
Figure 2.1.3	Tow arrangement and offsets	5
Figure 2.2.1	Processing sequence flowchart	9
Figure 2.2.2	Filters applied to raw data	10
Figure 2.2.3	Band pass filter parameters	9
Figure 2.2.4	Spherical divergence corrections	11
Figure 2.2.5	Geometry of shot and CMP gather	12
Figure 2.2.6	Velocity picking with Geodepth	13
Figure 2.2.7	Effect of different velocity picks	12
Figure 2.2.8	Initial velocity model	14
Figure 2.2.9	Final velocity model	15
Figure 2.2.10a	Stacked section (no migration)	16
Figure 2.2.10b	Stacked section (migrated)	17
Figure 2.2.11	Non-migrated vs. migrated comparison	18
Figure 3.0.1a	Gravity map of northeast Pacific	22
Figure 3.0.1b	Gravity map of study area	23
Figure 3.1.1	Line 2	24
Figure 3.1.2a	Line 2: Southern end	25
Figure 3.1.2b	Line 2: Southern end with faults outlined	26
Figure 3.1.3	Line 2: Central section	27
Figure 3.1.4a	Line 2: Northern end trench	28
Figure 3.1.4b	Line 2: Northern end trench with sediments outlined	29

Figure 3.1.4c	Line 2: Northern end trench with faults outlined	30
Figure 3.2.1	Line 12E	31
Figure 3.2.2a	Line 12E: Eastern end	32
Figure 3.2.2b	Line 12E: Eastern end with sediments outlined	33
Figure 3.2.2c	Line 12E: Eastern end with faults outlined	34
Figure 3.2.3	Line 12E: Central section	35
Figure 3.2.5	Line 12E: Western end	36
Figure 4.1.1	Lines 3, 4, 5, 6	40
Figure 4.1.2	Magnetic anomaly map	41
Figure 4.1.3	Earthquake distribution map	42

## **ABSTRACT**

The largest earthquakes in the world occur at subduction megathrusts, posing a great hazard to coastal communities. Seismicity in these subduction zones behaves differently along the margin and is in part controlled by faulting of and sedimentation thicknesses on the subducting plate, and by the bathymetry and geometry of the down going portion of the lithosphere. All these factors differ along the strike of the margin resulting in different patterns of seismicity observed regionally. The geometry of the down going plate refers to pre-existing structures such as seamounts and bending faults, caused by the bending of the plate as it plunges under the continental lithosphere. Variations in the faulting and hydration of the outer rise have strong correlations to variations in seismicity at depth, with greater amounts of deformation and hydration leading to earthquakes through dehydration embrittlement or reactivation of faults. Also, more uneven plate surfaces are more likely to form small asperities upon subduction, leading to interplate seismicity. It is therefore of importance to understand the characteristics of the subducting lithosphere to better understand seismic hazards along a subduction thrust.

## **LIST OF ABBREVIATIONS USED**

CMP: Common mid point

MCS: Multichannel seismic

NMO: Normal move out

TWT: Two way time (in seconds)

## **ACKNOWLEDGEMENTS**

I would like to extend my deepest gratitude to my supervisors Mladen Nedimović and Keith Louden, for providing me with an interesting thesis topic, and for all the assistance and support I needed to complete this thesis. I would also like to extend my gratitude to Harold Kuehn for all software expertise and patience. Your assistance is greatly appreciated.

## 1. INTRODUCTION

The project survey was carried out in the summer of 2011, covering the Alaskan Trench region offshore the Aleutian Island chain, with seismic data collected between Kodiak Island and Dutch Harbor (Figure 1.1.1) The survey was designed to image the locked zone on the megathrust, estimated areas of past rupture, and transition areas to stable sliding along the megathrust while also focusing on imaging structures on the downgoing plate including bending related normal faulting

The objective of this thesis is to produce clear images of the seafloor and shallow subsurface along lines 2 and 12E. The focus of the imaging will be aimed at the sediments and upper basement to identify any faulting, variation in sediment thicknesses, in addition to observing basement topography. All these factors influence the degree of plate coupling along the Alaskan megathrust subduction zone, and therefore serve as controls on seismic activity on the megathrust. Imaging completed along lines 2 and 12E will be compared to the other previously processed lines from the survey (Shillington et al., 2014) to observe variations along strike in the characteristics of the subducting Pacific plate, with the end goal to relate the varying pattern in seismic behavior along the margin to the variations in plate characteristics we observe along the margin.

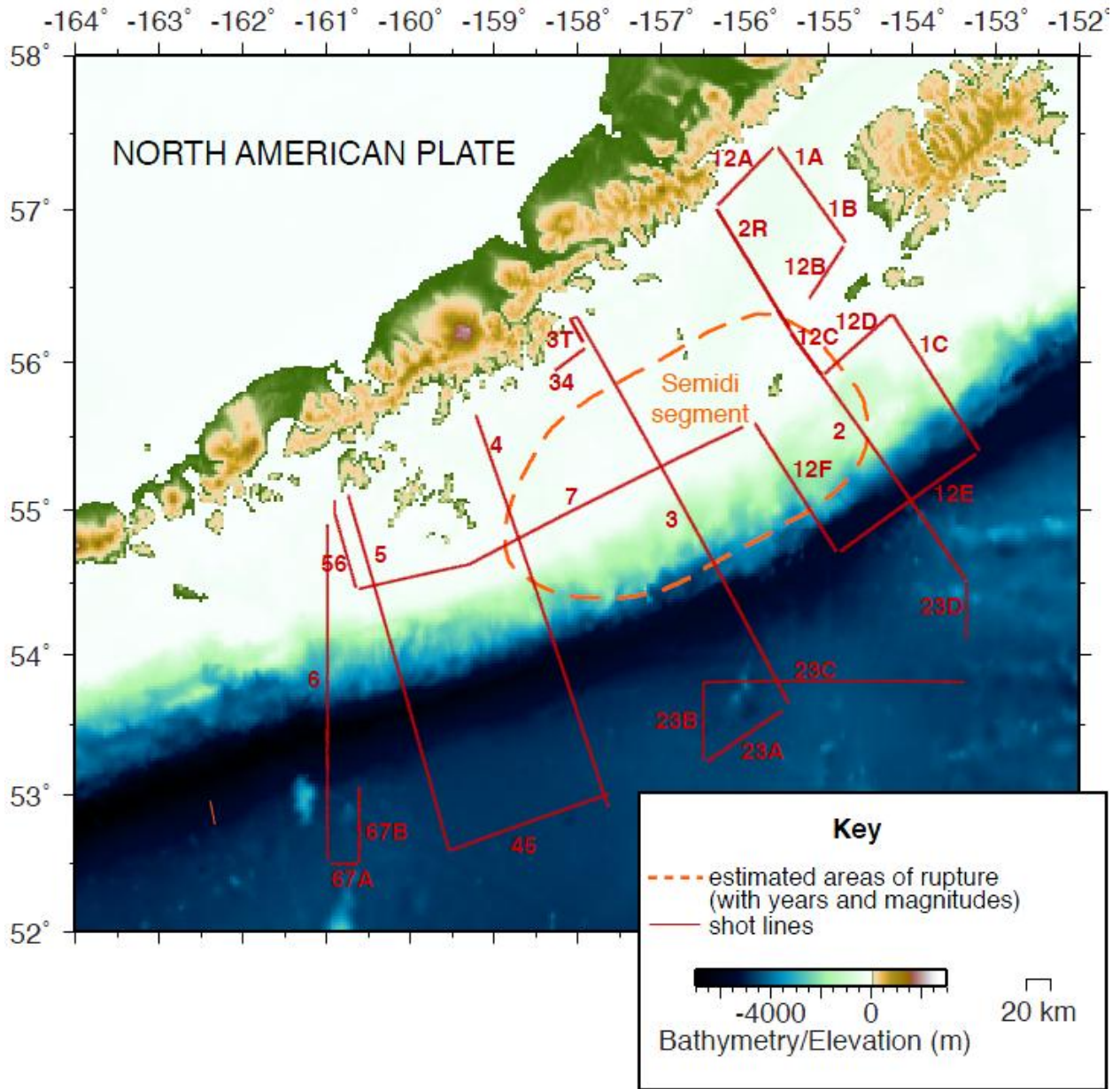


Figure 1.1.1: Study area map showing the lines along which seismic data was acquired

## **2. METHODS**

### **2.1. Data Acquisition**

The MCS data was acquired along the Aleutian trench during a survey in the summer of 2011. The research vessel, the Marcus G. Langseth, was equipped with an array of airguns (Figure 2.1.1) capable of releasing a total air volume of 108.15 L. Expansion of the air bubbles generates a pressure wave in the water, which reflects off the ocean floor and sub-seafloor structures, and is recorded by the 1272 channels along two 8 km long streamers (Figure 2.1.2 and 2.1.3). The air gun array was fired at 62.5 meter shot intervals while sampling at a rate of 2ms. The source and the port side streamer (streamer 2) were towed at 12 m depth and the starboard side streamer (streamer 1) was towed at 9 m depth. The deeper streamer was used with the goal of maximizing lower frequencies for improved deep imaging, while the shallower streamer served for better imaging of the sediments and upper crust. Towing two long streamers allowed for improved signal to noise ratio, with an expanded range of frequencies, as well as deeper imaging.

For line 2, both streamers were used to acquire data with a transverse separation of 225 m between the streamers. The starboard streamer, at 9 m depth, was towed 325.84 m behind the centre of the air gun source and the port streamer, at 12 m depth, was towed 235.68 m behind the centre of the source. During shooting, operations powered down twice due to the presence of marine mammals.

For line 12E, only the port side streamer (streamer 2) towed at 12 m was used to record data. The starboard side streamer was towed in the water, but only provided navigational data. (The streamers were towed with the same configuration as for line 2 described above.) The first portion of line 12E was shot only using half the air gun array as a source, while the other half was pulled in for maintenance. While shooting, operations had to be ceased and powered down

twice, due to the presence of marine mammals. Due to a temporary lock up of the acquisition system, shots 2838-2843 were missed.

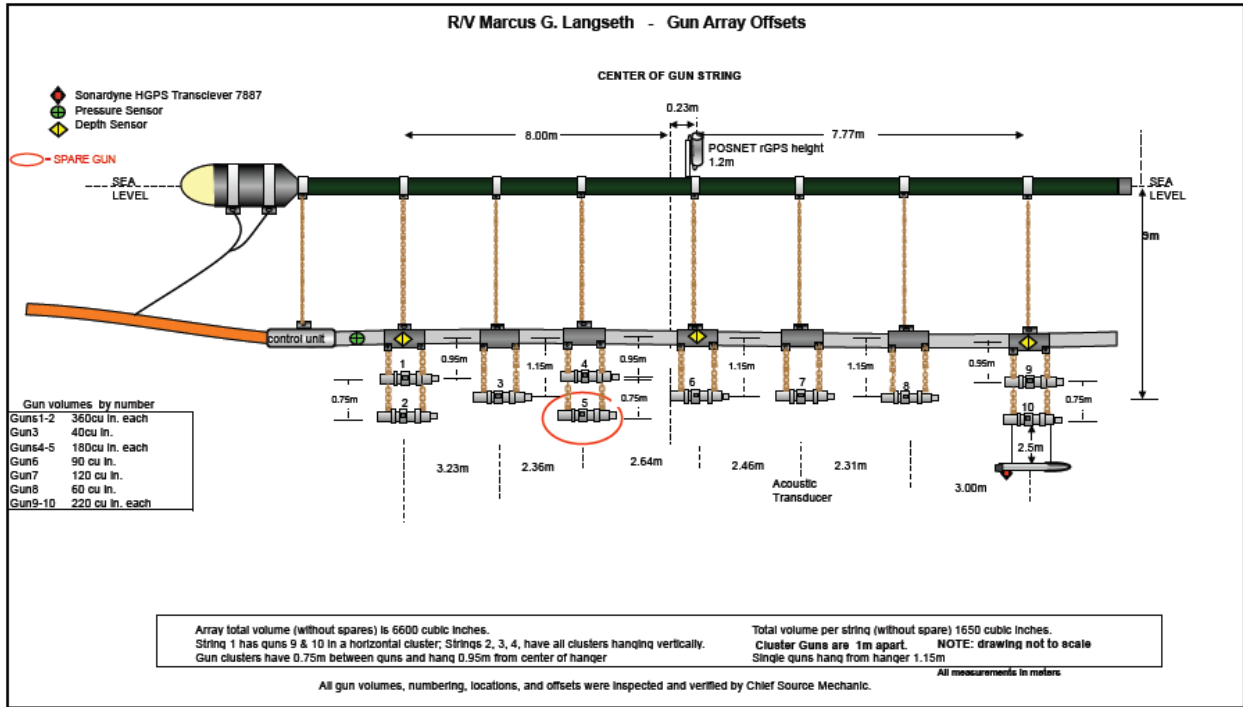


Figure 2.1.1: One string of the air gun array, showing depths and offsets of the air guns. Four of these strings were towed behind the vessel.

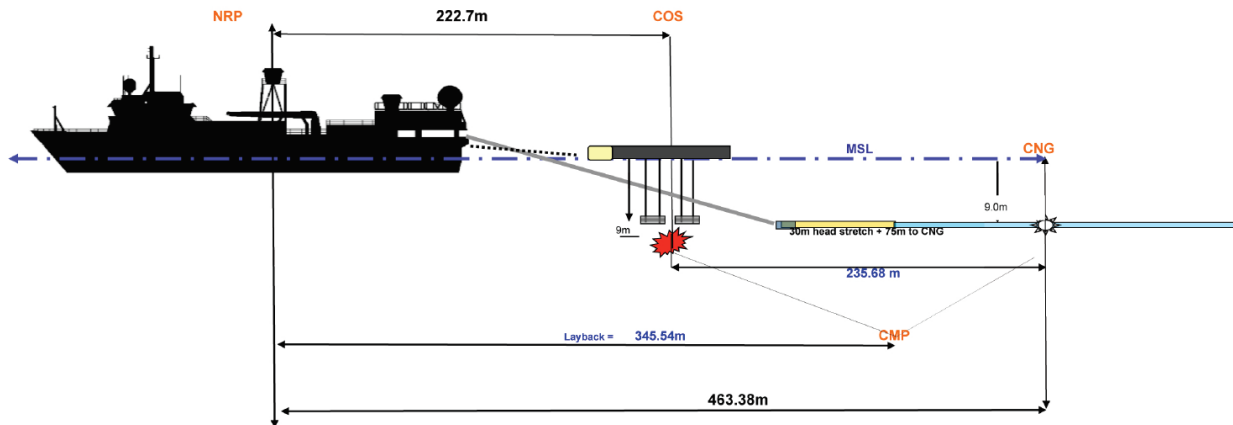


Figure 2.1.2: Offsets of the vessel, air gun array, and streamers relative to each other

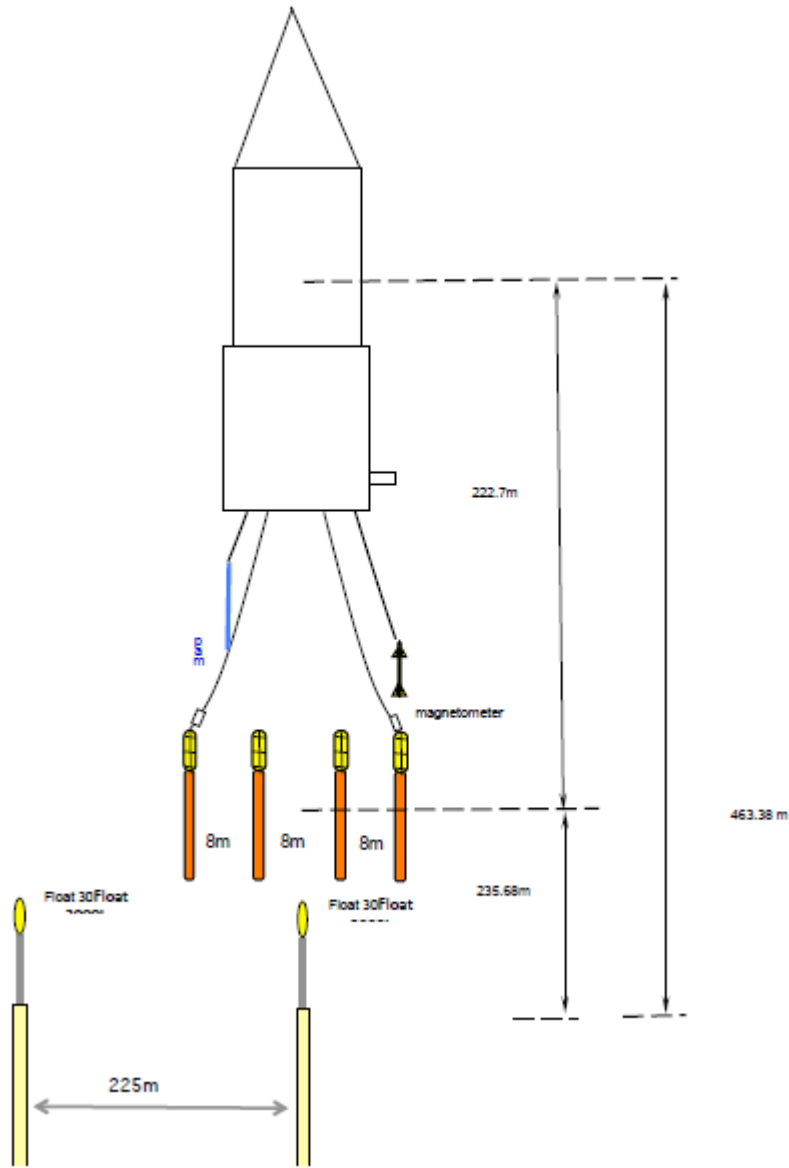


Figure 2.1.3: Arrangement of gun strings and streamers behind the vessel used for shooting line 2 and 12E

## 2.2. Data Processing

Processing of the data was carried out following a basic processing sequence outlined in Yilmaz, (2001) (Figure 2.2.1). Much of the preprocessing work, including the field geometry and demultiplexing of the data, had already been completed on board the survey vessel prior to receiving the data set. The first step taken was the editing of the initial raw shot gathers (see Figure 2.2.2a). Using Paradigm's Focus software the gathers were closely examined for dead or excessively noisy channels which were then removed from the data. After removal of unwanted traces, steps were taken to remove much of the unwanted noise from the data in order to improve the signal to noise ratio. First a module called FILTER was used to apply a band-pass filter the data. This is a filter which passes frequencies within a chosen range while attenuating frequencies which lay outside the range. (See Figure 2.2.3) It takes four frequencies as parameters; F1, F2, F3, F4. F2 and F3 define the range of frequencies which are to be passed in full. F1 and F4 are the values at which no frequencies below and above, respectively, are to be passed. The area between F1 and F2 and between F3 and F4 is a taper zone. The band-pass filter for this data was designed to attenuate the low frequency signals associated with swell noise introduced by ocean wave action at the surface. The values 2, 6, 200, 220 were chosen as optimal values to attenuate the low frequency swell noise, while passing all desired higher frequencies (see Figure 2.2.3b).

Following the band-pass filter in the sequence, the module GAIN was used to apply a spherical divergence correction to the shot gathers. This correction is necessary to boost the amplitudes at later times (greater depths), correcting for the loss of signal with increasing travel time/distance due to the spherical spreading and dissipation of energy as it propagates through the Earth's subsurface. The GAIN module offered the option of applying an offset dependant spherical divergence correction or an offset independent spherical divergence correction. The

offset dependant spherical divergence correction was selected due to a recovery of greater signal strengths at further offsets than the offset independent correction (see Figure 2.2.4). In order to apply the spherical divergence corrections properly a velocity model is required to provide correct velocities for the corrections. Thus the GAIN module was not added into the processing sequence until after the picking of velocities (described below).

Following the band-pass filter in the sequence, a module called SUPPRES was applied to compliment the band-pass filter in removal of swell noise. SUPPRES carries out time-variant, band-limited noise suppression targeting organized noise on seismic traces (ground roll, swell noise, air blasts, etc). The seismic trace is decomposed into noise and signal components by frequency filtering, based on what frequency band the user has input as noise, in this case a range of 0-6 Hz. The envelopes for noise and signal are calculated and then compared. The time windows where the noise exceeds the signal level are determined and in these windows the noise component is scaled down to the level of the signal. The two separated components of the data, the signal trace and the noise trace (which has now been scaled down) are then summed to yield the final result (see Figure 2.2.3d).

The module AMPSCAL was applied following the FILTER and SUPPRES modules to attenuate bursts of noise which can be attributed to jerking of the tail buoy or cable while the array was being towed behind the vessel. Using AMPSCAL the data is analyzed across small overlapping windows. It compares the window amplitude with the amplitude of the corresponding window on the adjacent traces in the dataset. The windows containing anomalously high amplitudes are scaled down (see Figure 2.2.3e).

After editing and improving the signal in the shot gathers, the shot gathers were sorted into common midpoint (CMP) gathers for further processing. In a shot gather each gather of traces is a result of a single shot recorded across many receivers. There is one shot gather for

each shot fired during data acquisition. The data in the shot gathers can be resorted by surface geometry to take data from different shots and receivers associated with a single reflection point in the sea bed (see Figure 2.2.5).

Once the data was sorted into CMP gathers it could be imported into Paradigm's Geodepth software for velocity picking. The software displays the CMP gather selected and shows a corresponding velocity vs time field of calculated semblance values (see Figure 2.2.6). Velocities are picked for a number of reflections/layers in the CMP gather by selecting velocities in regions of high semblance, while aiming to flatten the reflectors which are initially parabolic in shape. This process (NMO) is essential to correct for time delays in signal arrival time at receivers of increasing offset distance. The correction must be made to bring traces of varying offsets to the same arrival times in order for accurate summing for stack production. Picking too high a velocity results in an under-correction with the parabola dipping downward whereas picking too low a velocity results in an over-correction with the parabola dipping upwards (see figure 2.2.7). When proper velocities are picked the reflections in the CMP gather should all appear perfectly horizontal. The velocities were picked for the sediment layers overlying the crystalline basement rock with the first velocity pick corresponding to the seabed reflector and the final velocity picked corresponding to what was best guessed as the basement reflector. Once velocities were picked the data was exported back to Focus to create a velocity model which could be used for further processing of the data (see Figure 2.2.8). After a stacked section was created (described below) it was imported to Geodepth and displayed alongside the CDP gather and semblance display. This allowed for more accurate velocity picks for the basement reflector now that the location of the reflector corresponding to the basement is perfectly clear in the stack. After the completion of velocity picking for the sediment standard ocean crust velocities were hung off the top basement pick for a more complete and regionally accurate velocity model.

Once NMO has been applied a stack can be produced. The STACK module sums seismic traces, outputting a single trace for each input ensemble of traces and resulting in a stacked section depicting a two dimensional slice of the subsurface along the surveyed line (see Figure 2.2.9). This is a very effective method for improving signal to noise ratio of the MCS data.

Finally, once a stacked section was completed, Focus's MIGTX module was used to apply migration to the stacked section. This process has the aim of collapsing diffractions, which are caused by sharp edges or obstacles in the subsurface, and moving dipping interfaces to their correct position to produce a more accurate final image. MIGTX applies Kirchoff migration (which uses the integral form of the wave equation) to apply back-propagation of the seismic wave field from the region where it was measured, into the region to be imaged (Figure 2.2.10). (Figure 2.2.11 provides a closer look at the effect of migration.) As can be seen in the figures, the inverse parabolic forms which are present in the non-migrated section are removed in the migrated section, and the dips of the seamount features have steepened to a more accurate dip.

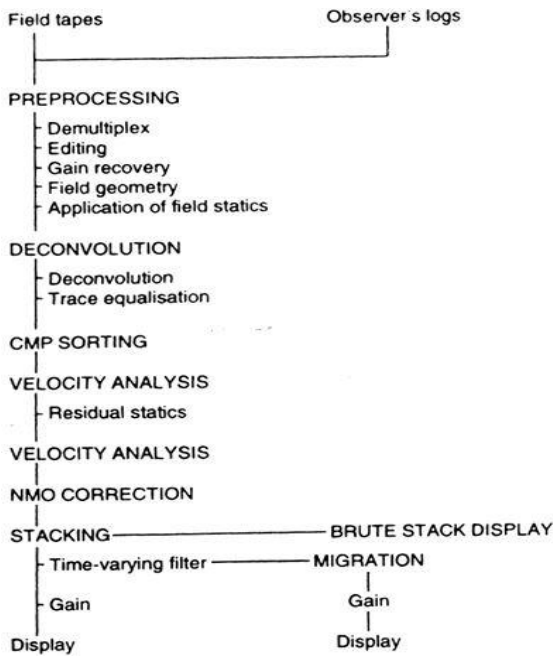


Figure 2.2.1: Basic processing sequence (After Yilmaz, 2001)

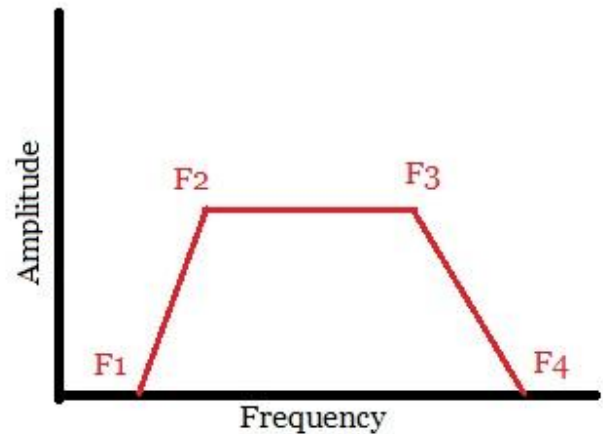


Figure 2.2.3: Bandpass filter. The bandpass filter specific to this project had F1, F2, F3, F4 values of 0, 6, 200, 220 respectively

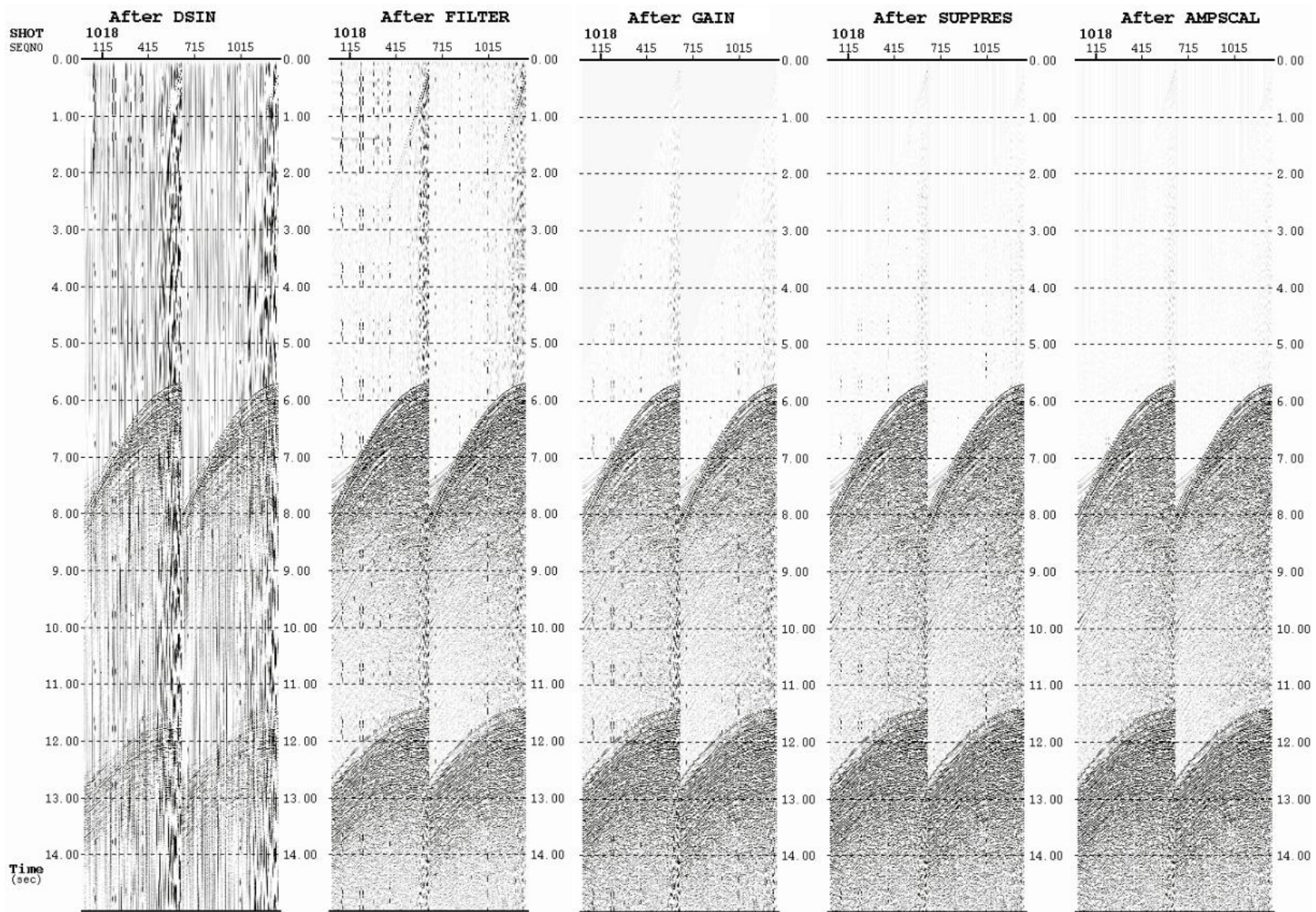


Figure 2.2.2: Filters used. (a) Raw shot gather (b) After band pass filter was applied (c) After spherical divergence correction was applied (d) After SUPPRES module was applied (e) After AMPSCAL module was applied

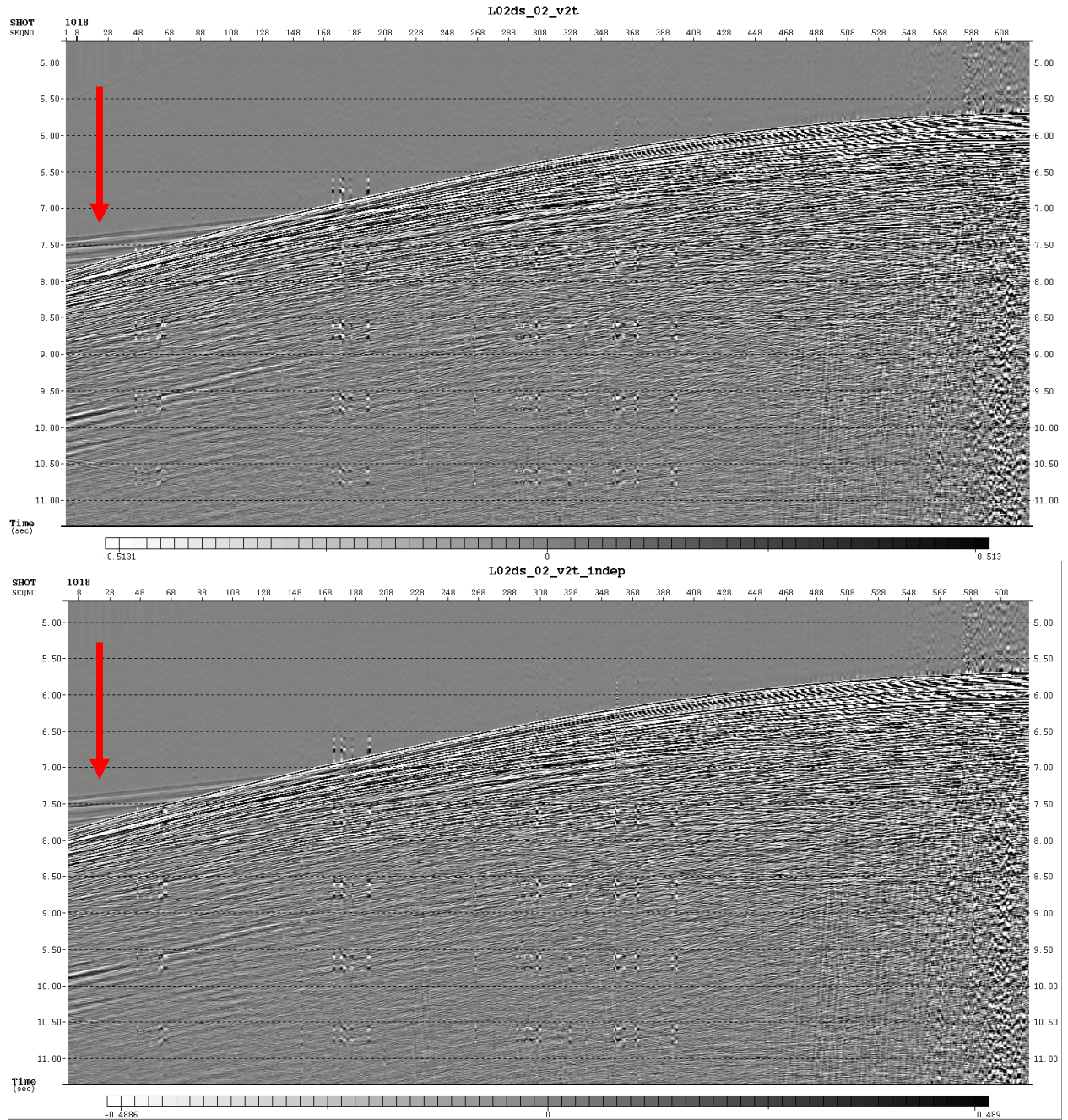


Figure 2.2.4: Offset dependent spherical divergence correction (top) and offset independent spherical divergence correction (bottom). Late arrivals are stronger for the offset dependent correction (top).

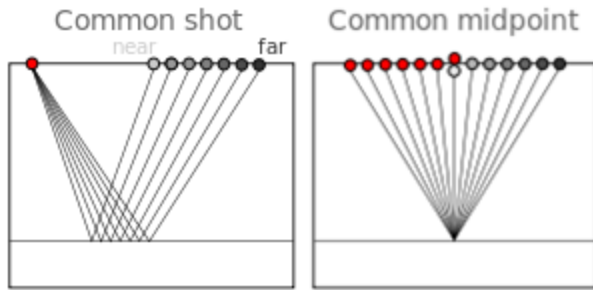


Figure 2.2.5: Geometry of a shot gather (left) vs a CMP gather (right) (After agilegeoscience.com).

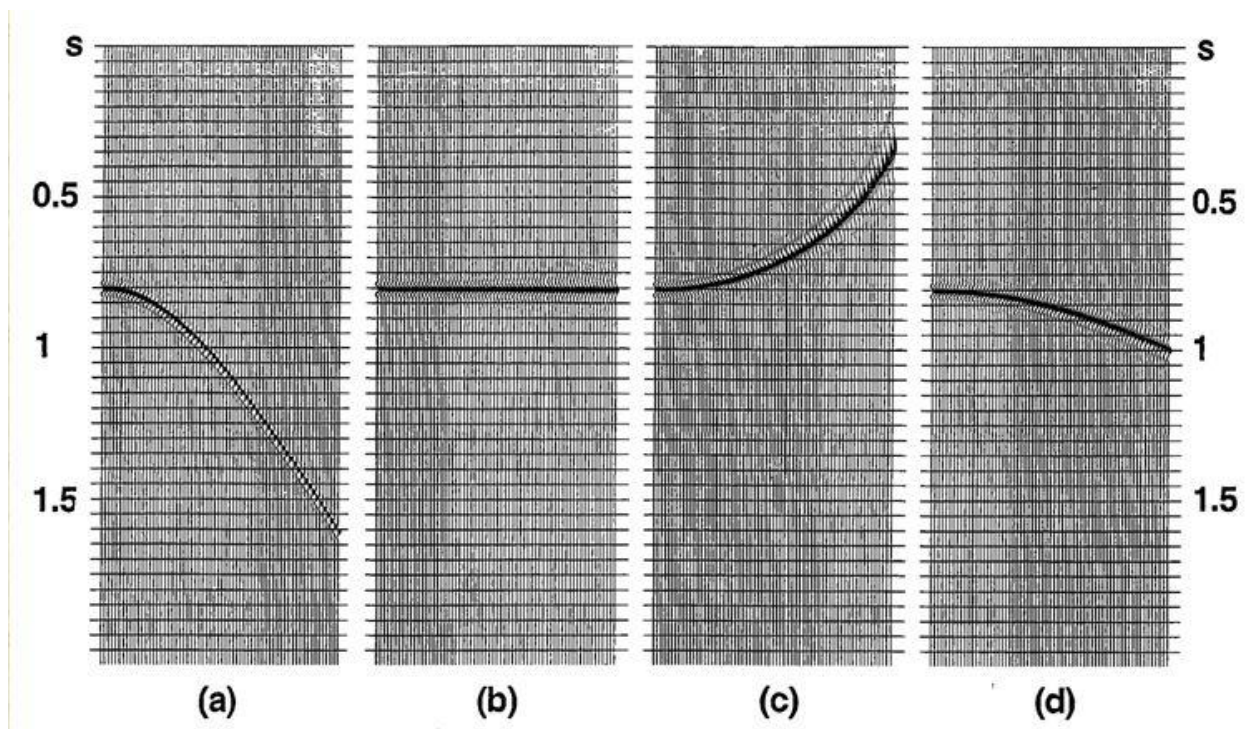


Figure 2.2.7: Picking velocities (a) Original gather (b) Perfect correction, proper velocity picked (c) Overcorrection, too low a velocity picked (d) undercorrection, too high a velocity picked (After Yilmaz, 2001)

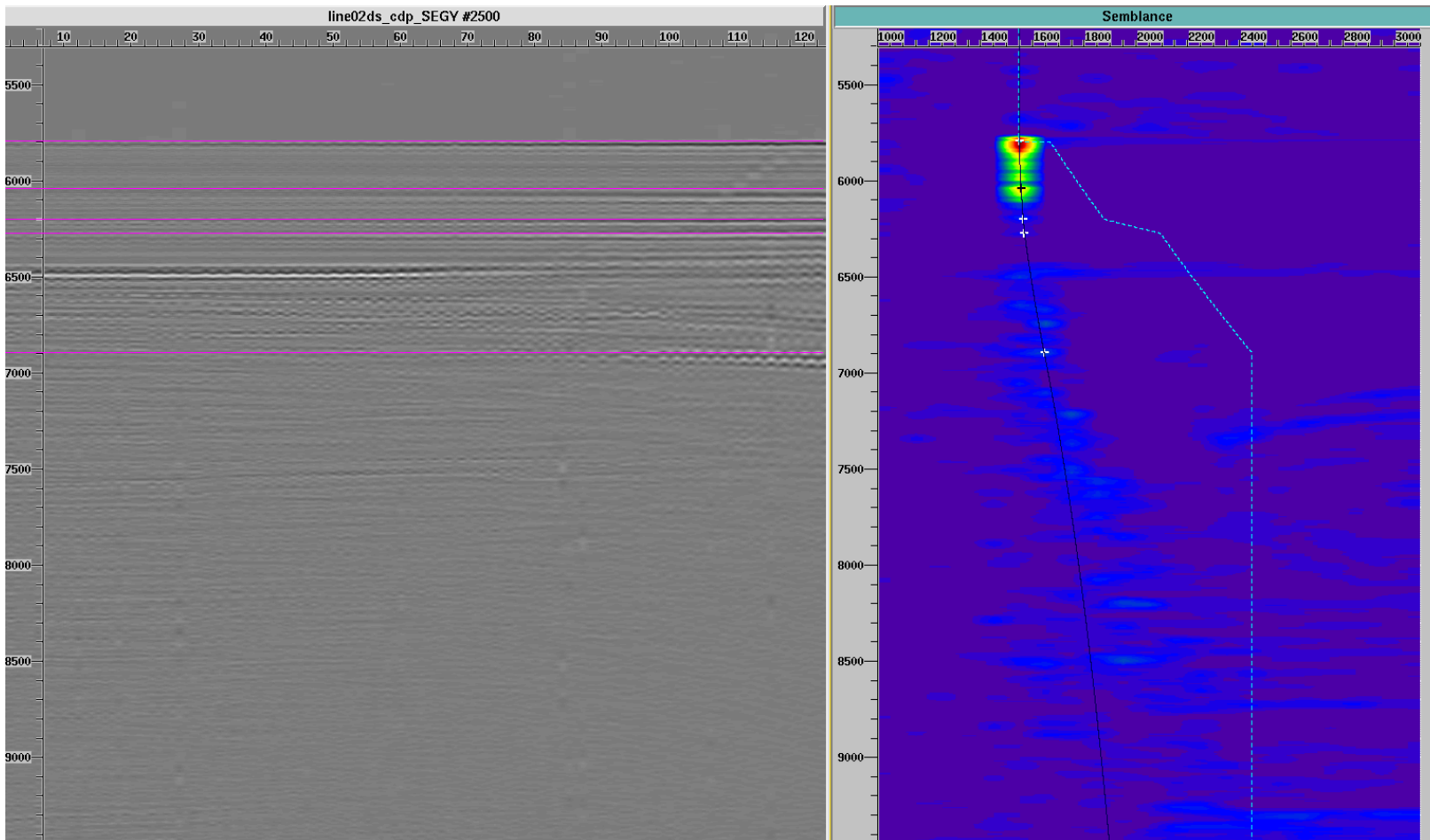
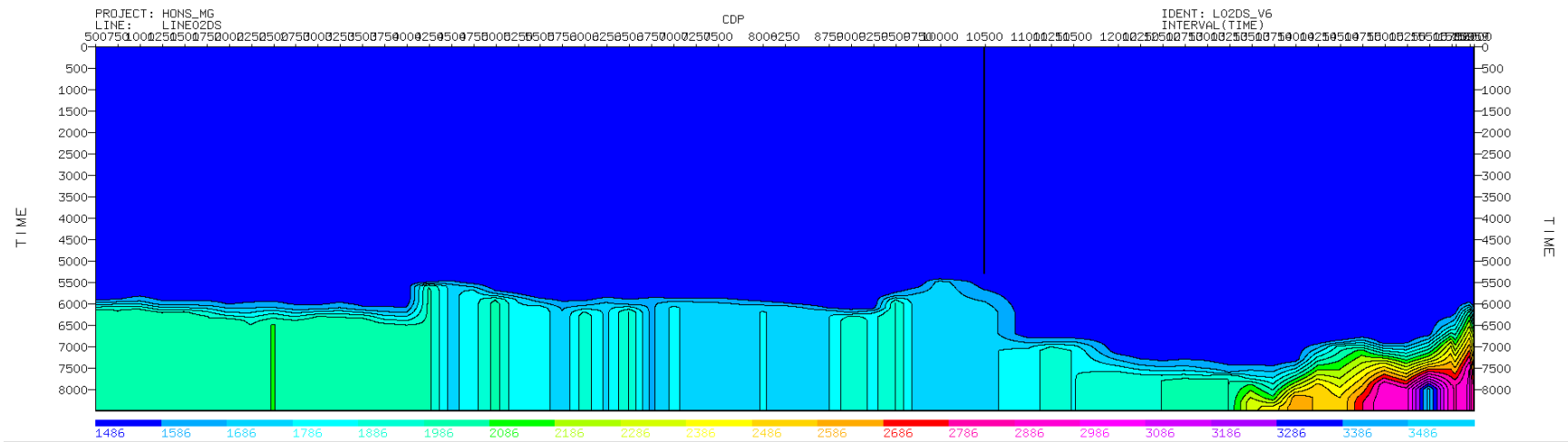


Figure 2.2.6: Picking velocities with Paradigm Geodepth software. Velocity picks are chosen in regions of high semblance (left) with the aim of flattening reflections (right). The semblance spectra ranges from cooler to warmer colors with warmer colors indicating higher degrees of semblance.





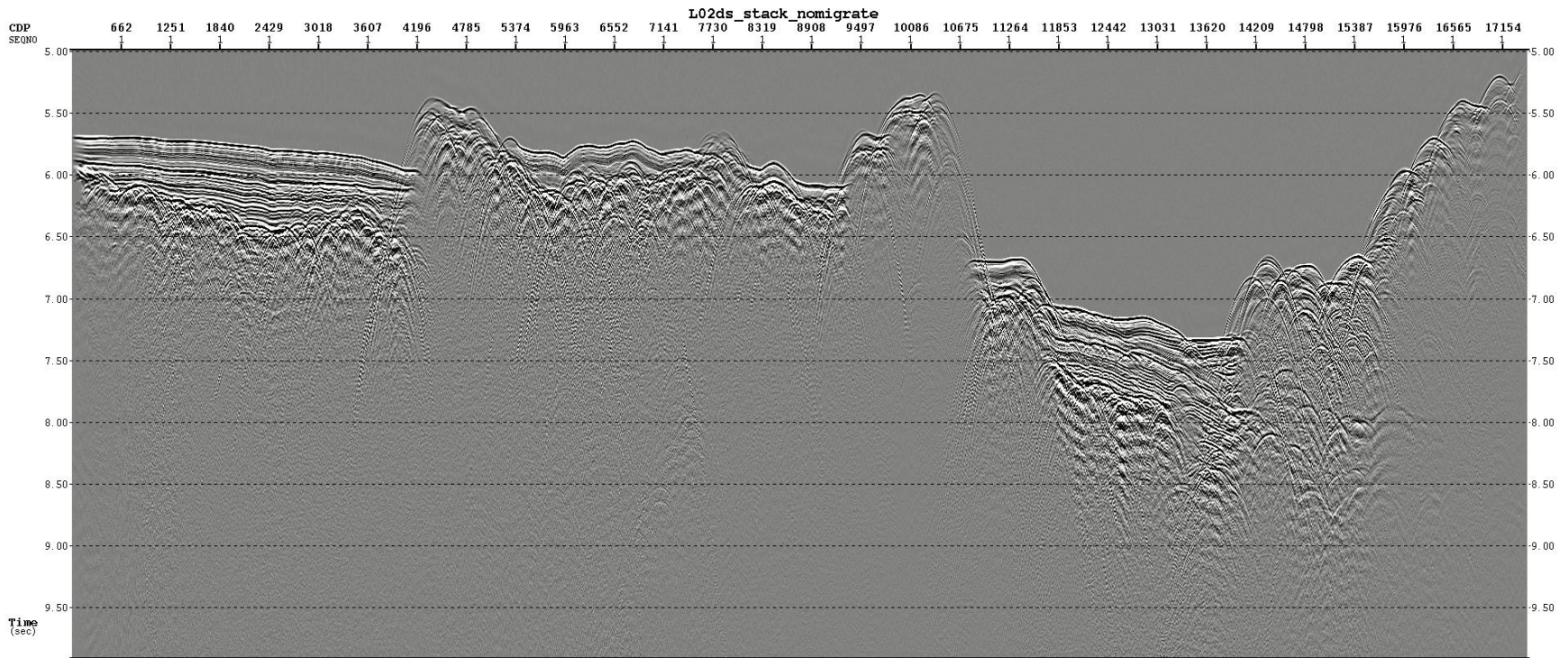


Figure 2.2.10a: Stacked section (no migration applied). Note the inverted parabolic nature of much of the structures shown due to diffractions resultant from the uneven basement structure.

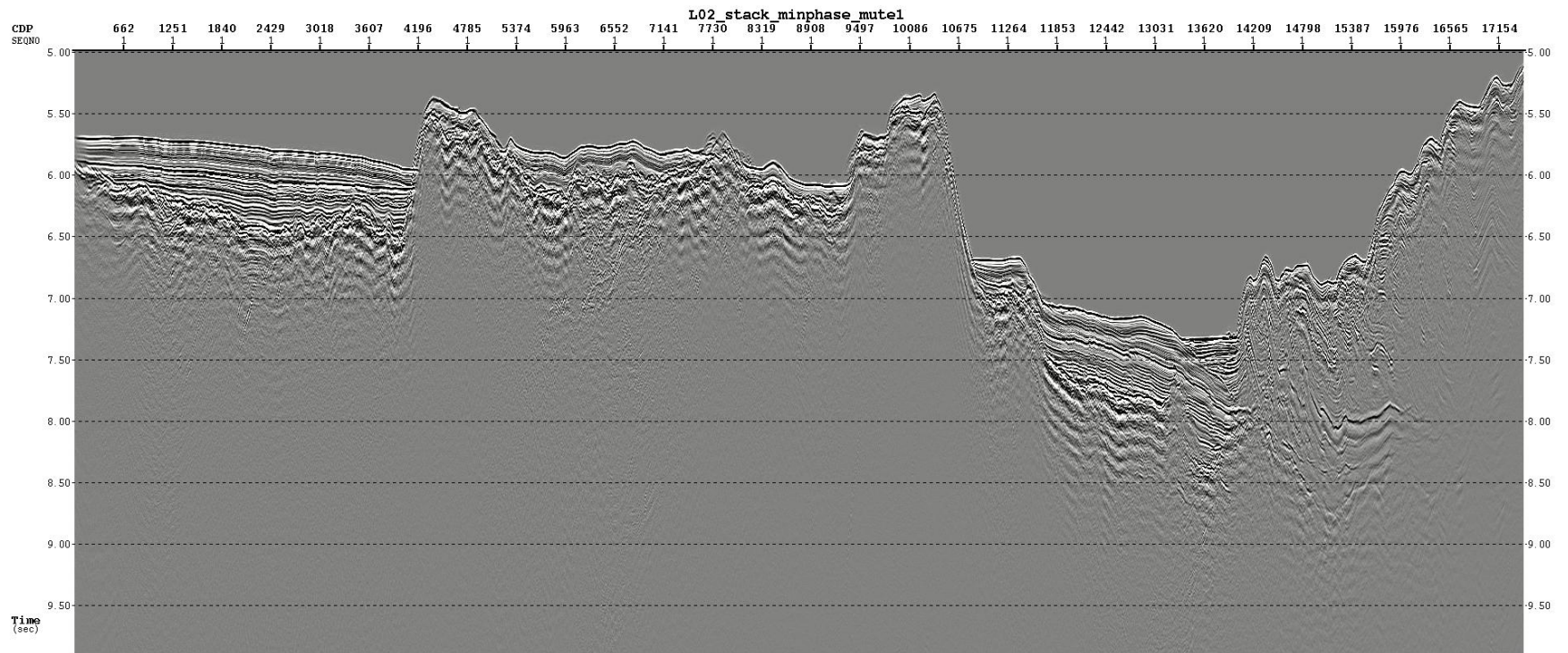


Figure 2.2.10b: Stacked section (with migration applied). Parabolic forms have been removed as dipping reflectors have been moved to their true positions and diffractions collapsed.

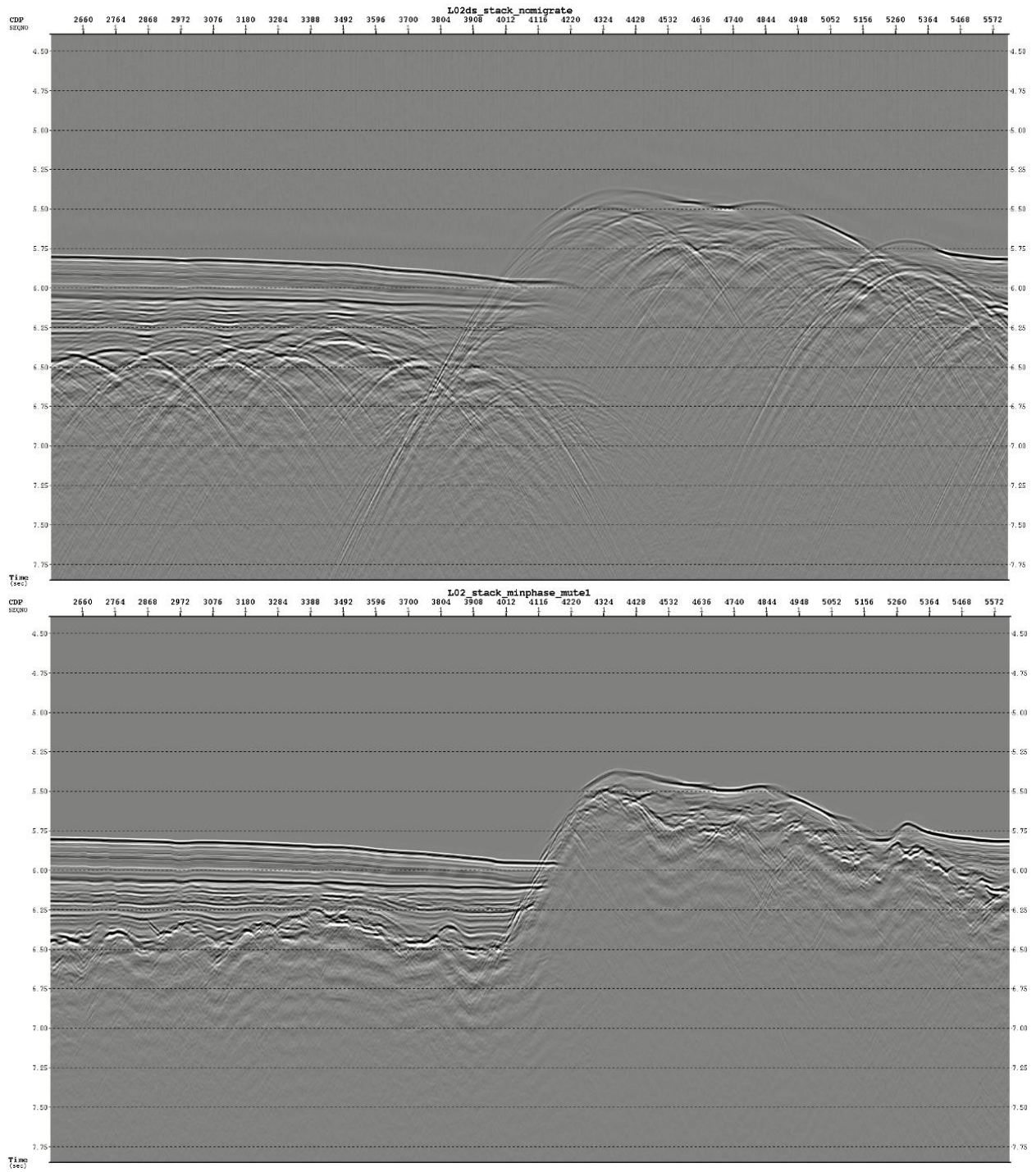


Figure 2.2.11: Comparison between the stacked section with no migration applied (top) and with migration applied (bottom)

### **3. RESULTS**

Line 2 runs perpendicular to the Alaskan Trench (Figure 3.0.1), imaging the ocean floor and subsurface in the trench to about 80 km seaward of the trench. The main structures we are looking for and expect to observe here include the degree of sedimentation, bending faulting (activated by plate bending at the outer rise), and plate topography such as seamounts (which can be seen on Figure 3.0.1).

Line 12E was shot trench parallel within the trench (Figure 3.0.1). The focus here is to examine the lateral variability in the degree of accumulated trench sediments which could help correlate the variable pattern of seismicity along the margin. Any faulting visible on this profile would indicate fault orientations oblique to the trench orientation.

#### **3.1. Line 2**

The deep sea portion of line 2 processed (Figure 3.1.1) shows a relatively rough seabed with two pronounced bathymetric highs approximately 22 km and 55 km seaward of the trench. These seamounts rise about a kilometer above the seafloor basement and appear to correspond with a ridge visible on the bathymetry and gravity map (Figure 3.2).

Focusing on the most southeast portion of line 2 (Figure 3.1.2a) we see a relatively thick accumulation of flat lying sediment over the basement, broken by the first bathymetric high. The sediments are on the order of about 550 m thick. Although the sediments are very flat lying, some minor deformation can be observed (Figure 3.1.2b). Looking closely we observe many faults spaced as closely as half a kilometer apart. Fault offsets here are relatively small with maximum offsets of < 30 m, and most of the observed faults having smaller offsets. Offsets in the sediment can be observed from depth all the way to the surface sediment layers, indicating

the faulting seen here occurred recently before additional sediment could accumulate above the faulted surface (with information on sedimentation rates in the area, faults could be accurately dated based on accumulation of sediment above the faulted surface).

In the central portion of line 2 (Figure 3.1.3), from the first bathymetric high to the second (which is assumed to be the east-west trending ridge visible in Figure 3.0.1), the sediment cover is much thinner, with an uneven surface mirroring the topography of the underlying basement. The sediment in this section reaches maximum thicknesses of 200 m, with much of the sediment cover even more thin. The sediment thins in the centre to a point where we observe outcropping of the basement rock. Structure in the image becomes unclear at this basement outcrop due to diffractions caused by the outcrop adjacent to the point which this line images. These diffractions were not able to be removed. No faulting could be observed across this central section.

The northwestern most portion of line 2 (Figure 3.1.4a) which images the trench area proves to be an area of key interest. Easily observable here (on the right of Figure 3.1.4a) are the landward dipping layers of previously accreted sediment forming the accretionary wedge. We see a large volume of sediments on the subducting Pacific plate being transported into the trench reaching a maximum thickness of 600 m. Two distinct packages of sediment can be observed (Figure 3.1.4b). First are the pelagic deep sea sediments running downdip into the trench, lying parallel with the subducting basement rock. These sediments are a result of marine depositional processes over the time spanning formation of the crust at the mid ocean ridge, to its subduction at the Aleutian trench. The second package of sediment does not lay in the same orientation as the subducting slab, but lay in horizontal drapes in the base of the trench. These are likely terrigenous sediments, derived from the erosional processes in Aleutian Islands, and the

continental mass overriding the Pacific plate at this location. Faulting can be clearly seen in the sediments (Figure 3.1.4c), and possibly the upper crust, with fault offsets observed on the scale of  $< 30$  m. However these fault offsets are extremely small when compared to other seismic lines collected further west (Shillington, 2014). The faulting on line 2 is small scale but extensive, occurring from the trench to the seaward limit of the seismic image about 85 km seaward of the trench. Top lying sediments in the trench do not show any sign of offset or deformation serving as an indication that the faulting seen near the trench did not occur recently.

### **3.2. Line 12E**

Line 12E (Figure 3.2.1) shot in and parallel the Aleutian trench gives a snapshot at the large lateral variability in sedimentation and basement topography along the trench which could have varying effects on seismicity. (Note that line 12E was shot from east to west.)

The eastern segment of line 12E (Figure 3.2.2a) shows a very thick accumulation of sediments in the trench, up to 1.25 TWT (estimated around 800 m thickness). In this area two distinct packages of sediment can be observed (Figure 3.2.2b): The lower sediments which are dipping gently eastward, roughly following the basement trend; and the upper sediments which lay completely horizontal, forming a cross cutting relationship with the lower sediments as you progress westward. As was the case observed in line 2, the lower sediments are likely pelagic sediment while the upper sediment package is probably of terrigenous origin from the landward (northern) side of the trench. In the lower sediment package, faulting with a small scale of displacement can be observed, on the scale of  $< 30$  m (Figure 3.2.2c). Since this profile runs parallel with the trench, any faults seen in this profile will have formed oriented obliquely to the trench.

The central portion of the line (Figure 3.2.3) shows two fairly sharp bathymetric highs spaced approximately 10 km apart and outcropping above the sediment cover. They are located approximately 5.5 km seaward from the trench. Sediment cover between the two seamount structures is much thinner than seen to the east, with the sediments showing a TWT of 0.5 s.

To the west of these outcrops (Figure 3.2.6) the basement is at a higher level than the east side of the line, and is covered in a relatively thin layer of sediments with a TWT maximum of 0.5 s, compared to the 1.25 s TWT observed on the western side. With the thinner sediment cover, the seafloor surface is rougher, with the sediments mirroring the rough basement topography, in contrast to the almost perfectly flat sea bed observed on the eastern segment (Figure 3.2.2a)

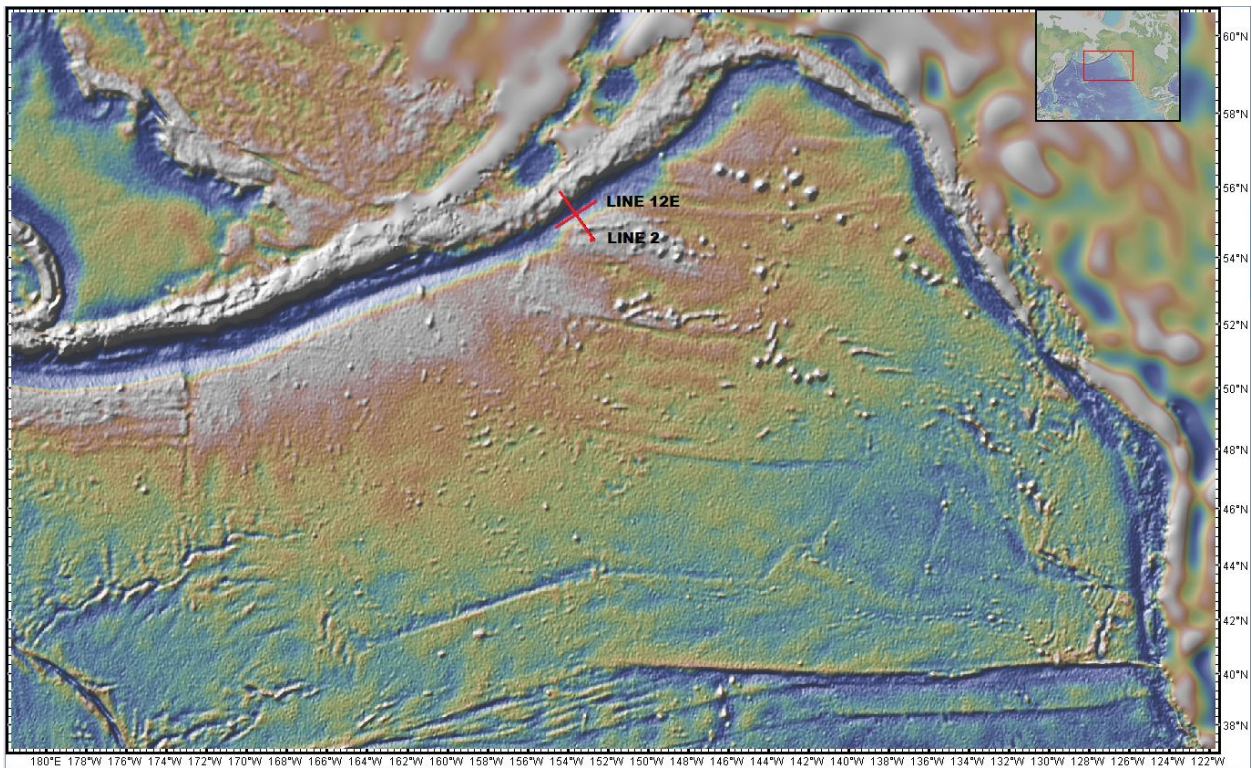


Figure 3.0.1a: Map showing gravity anomalies of the northeast Pacific. Cool to warm colors indicate gravity lows to highs which correspond to bathymetric lows to highs. Shown here is the gravity high along the seaward side of the trench resultant from flexure of the subducting plate

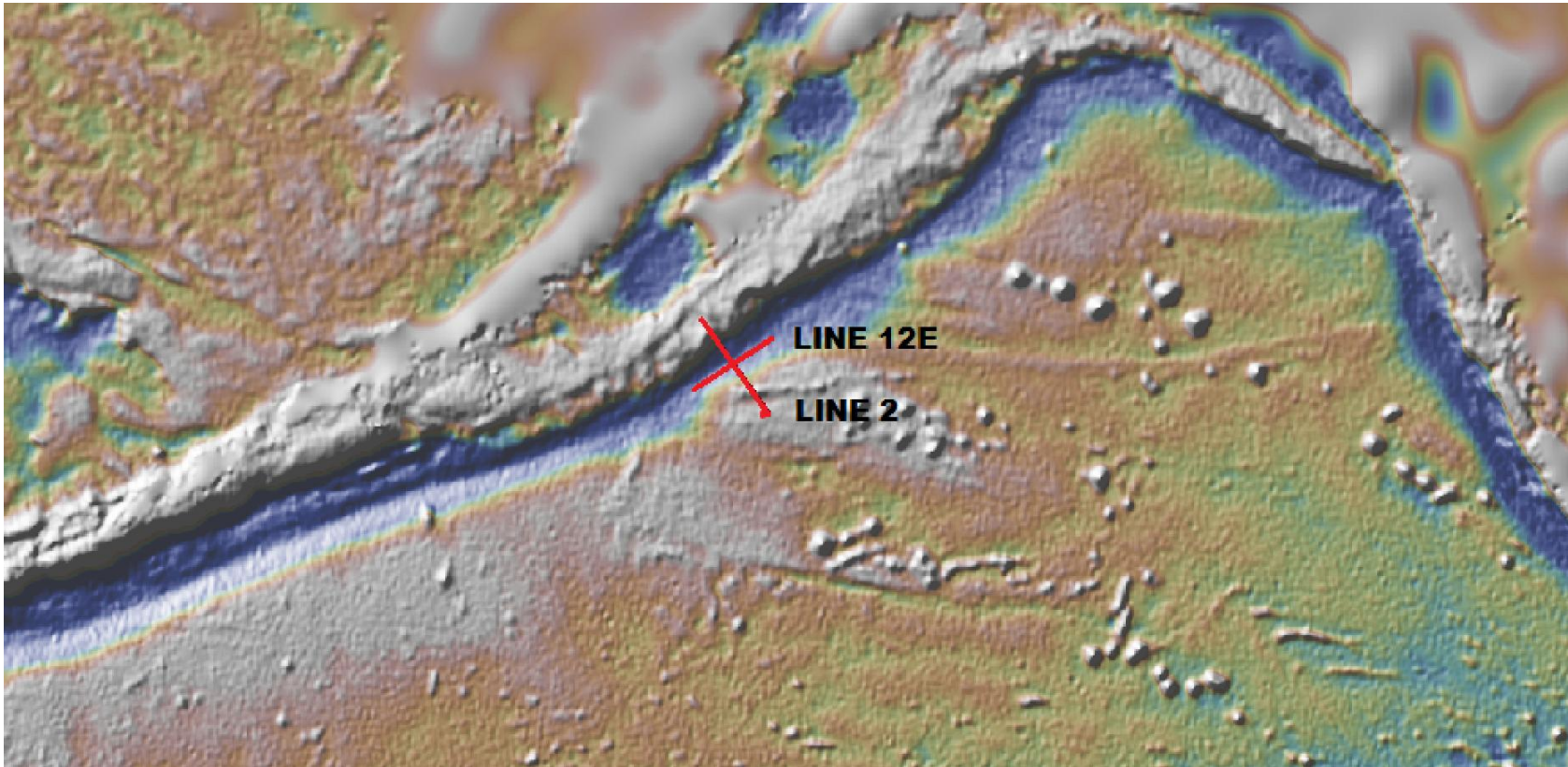


Figure 3.0.1b: Gravity map zoomed in to better show bathymetric features in the region where the seismic lines were shot.

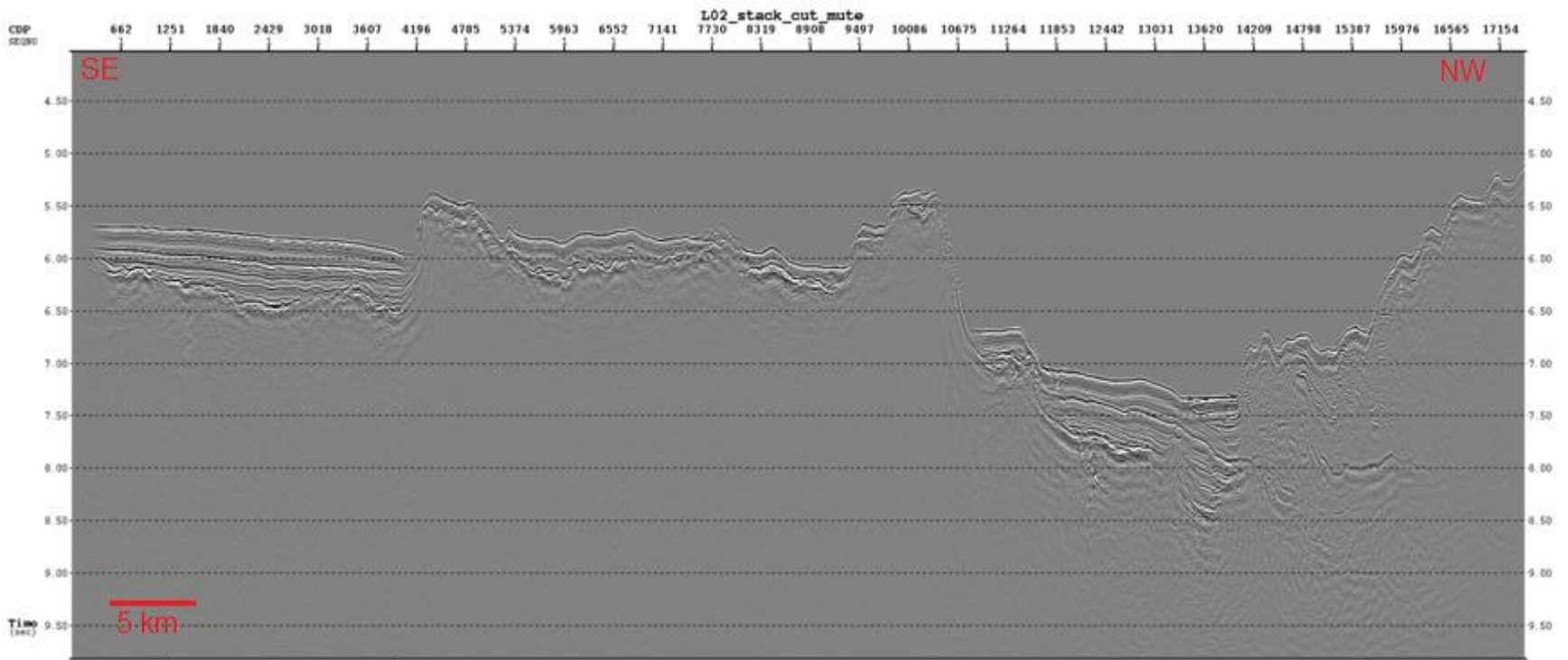


Figure 3.1.1: Line 2. Entire processed section showing the Pacific plate subducting into the Aleutian trench

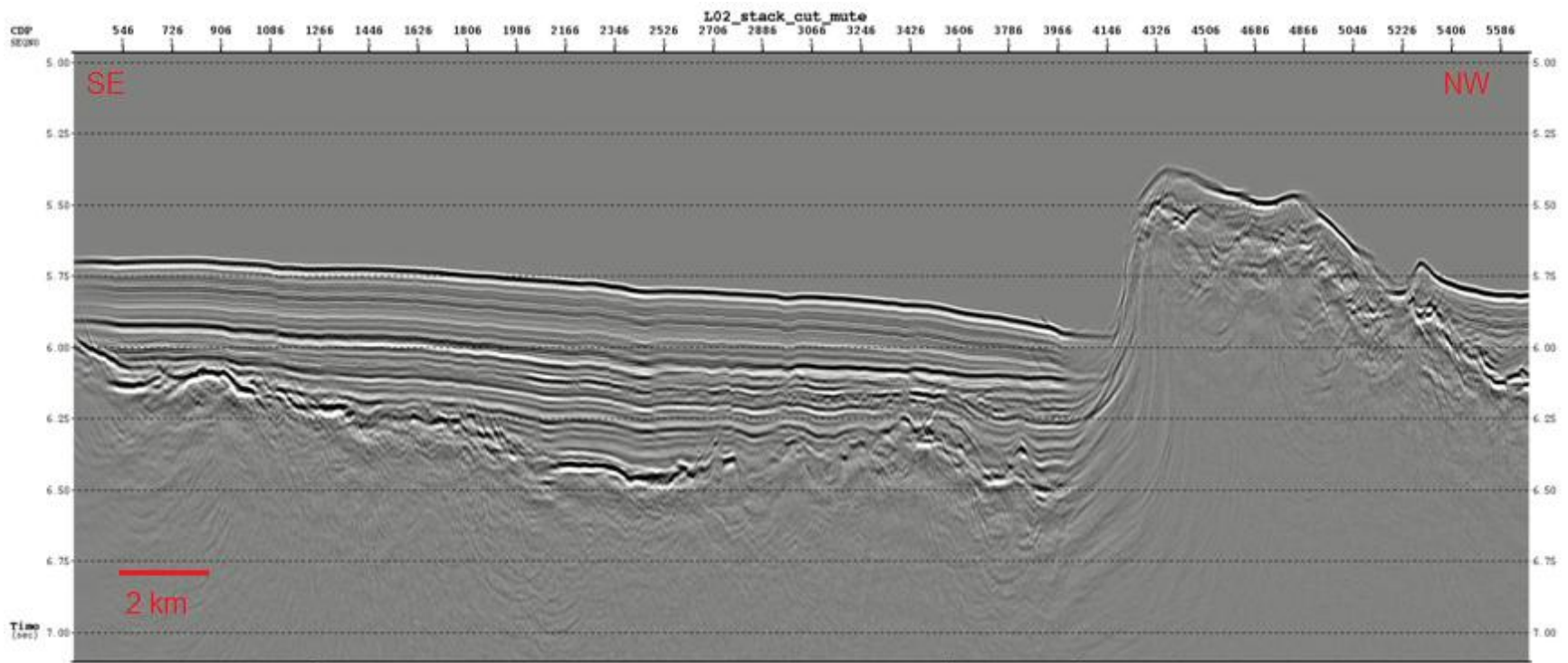


Figure 3.1.2a: Zoomed in section of left side of line 2 (furthest south of the trench). Relatively thick even sediment drapes are present until the first bathymetric high where the basement rises up rapidly.

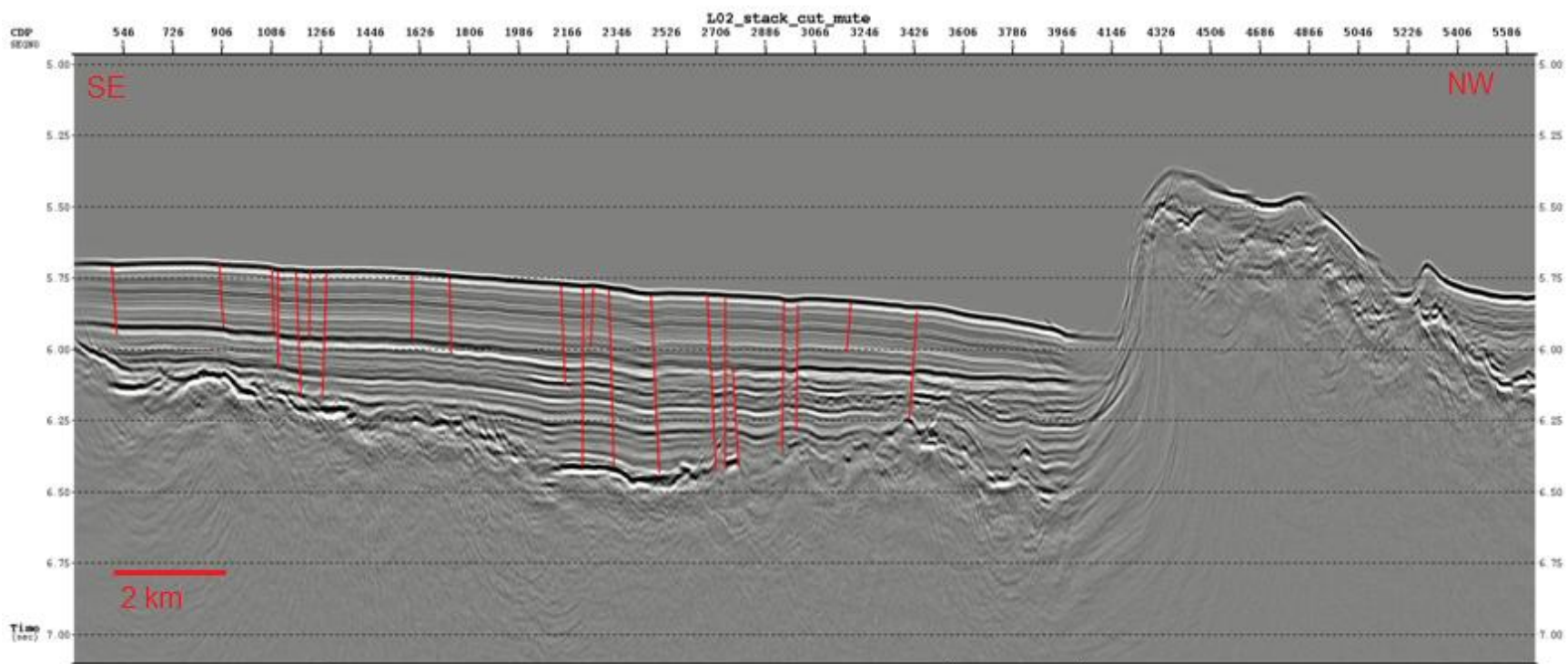


Figure 3.1.2b: Faults visible in sediments on the left (south) end of line 2.

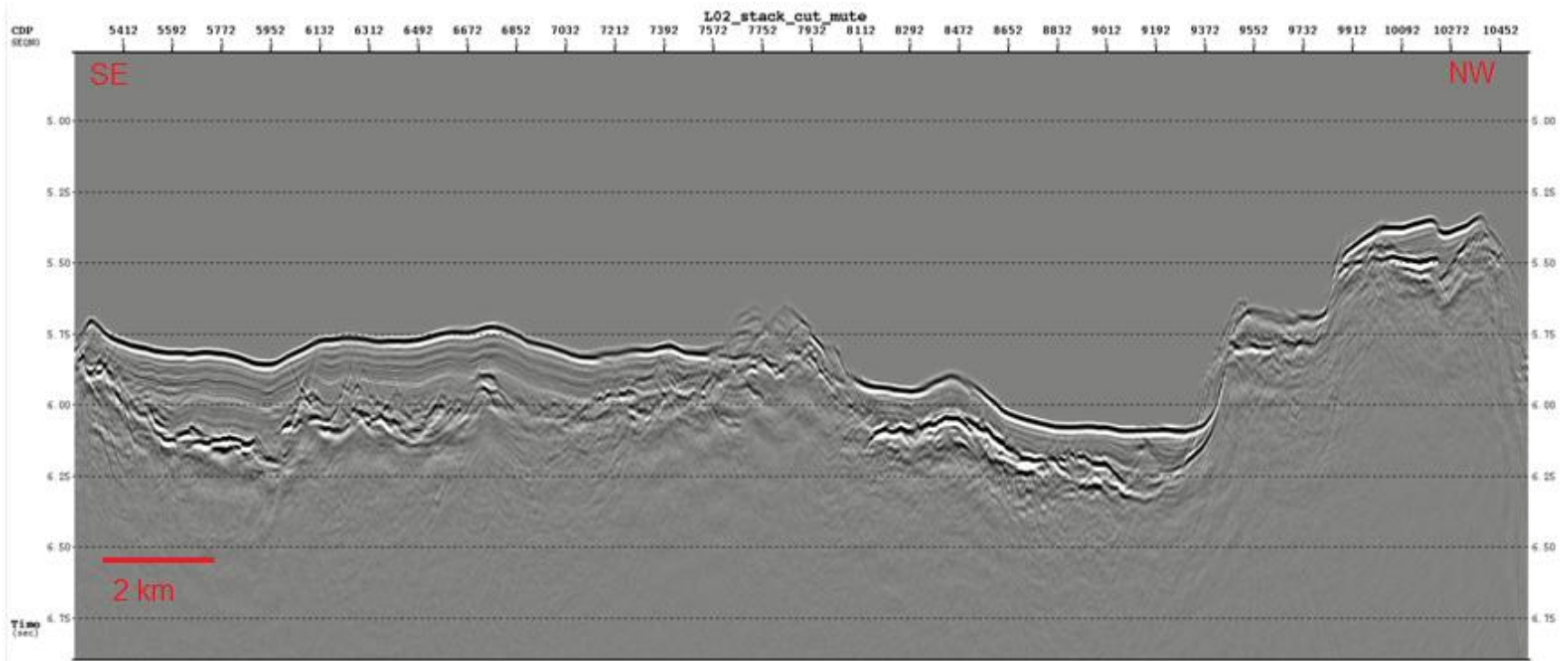


Figure 3.1.3: Zoomed in section of centre of line 2 (between the two bathymetric highs). Sediment cover is thin and follows basement topography. In the centre the basement outcrops with no sediment cover.

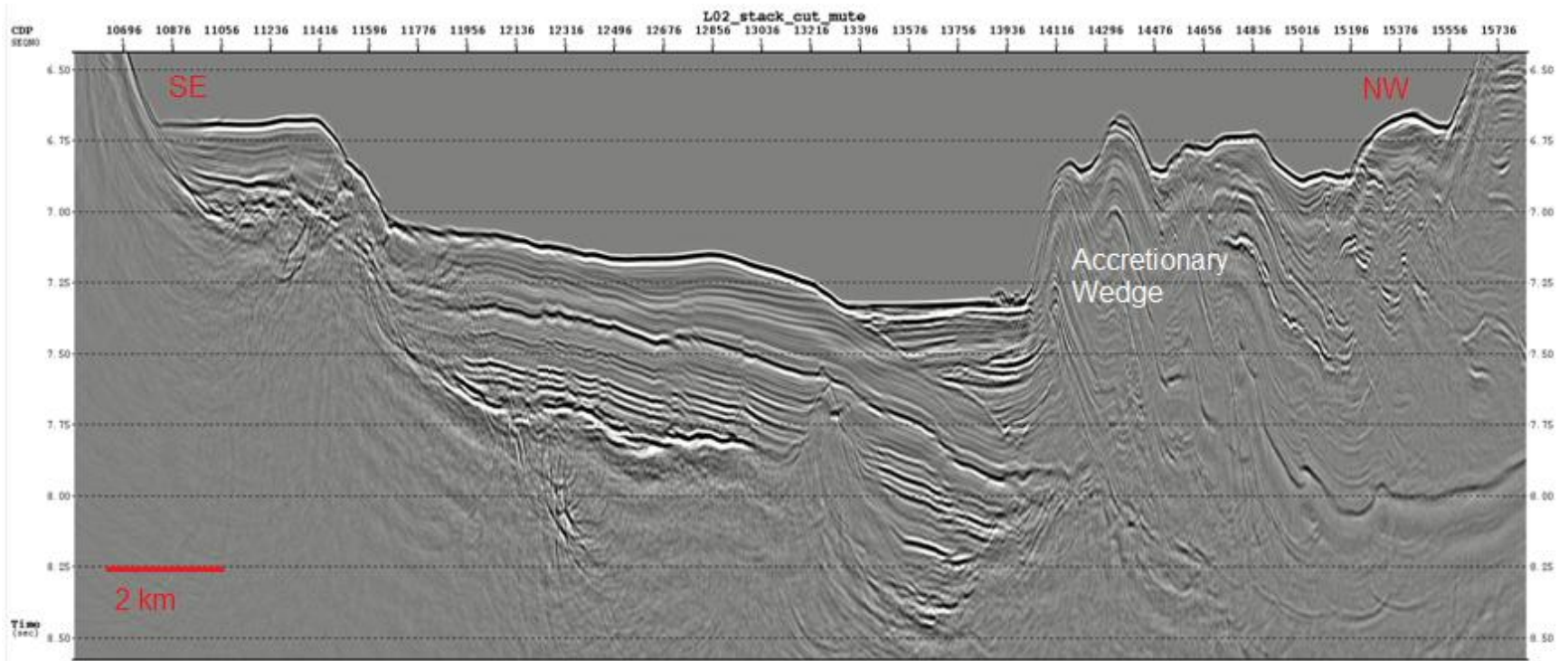


Figure 3.1.4a: Zoomed in section of the Aleutian trench on line 2 (furthest north on the line). Large volume of sediment is being carried into the trench. Easily visible are the landward dipping layers of accreted sediment forming the accretionary wedge.

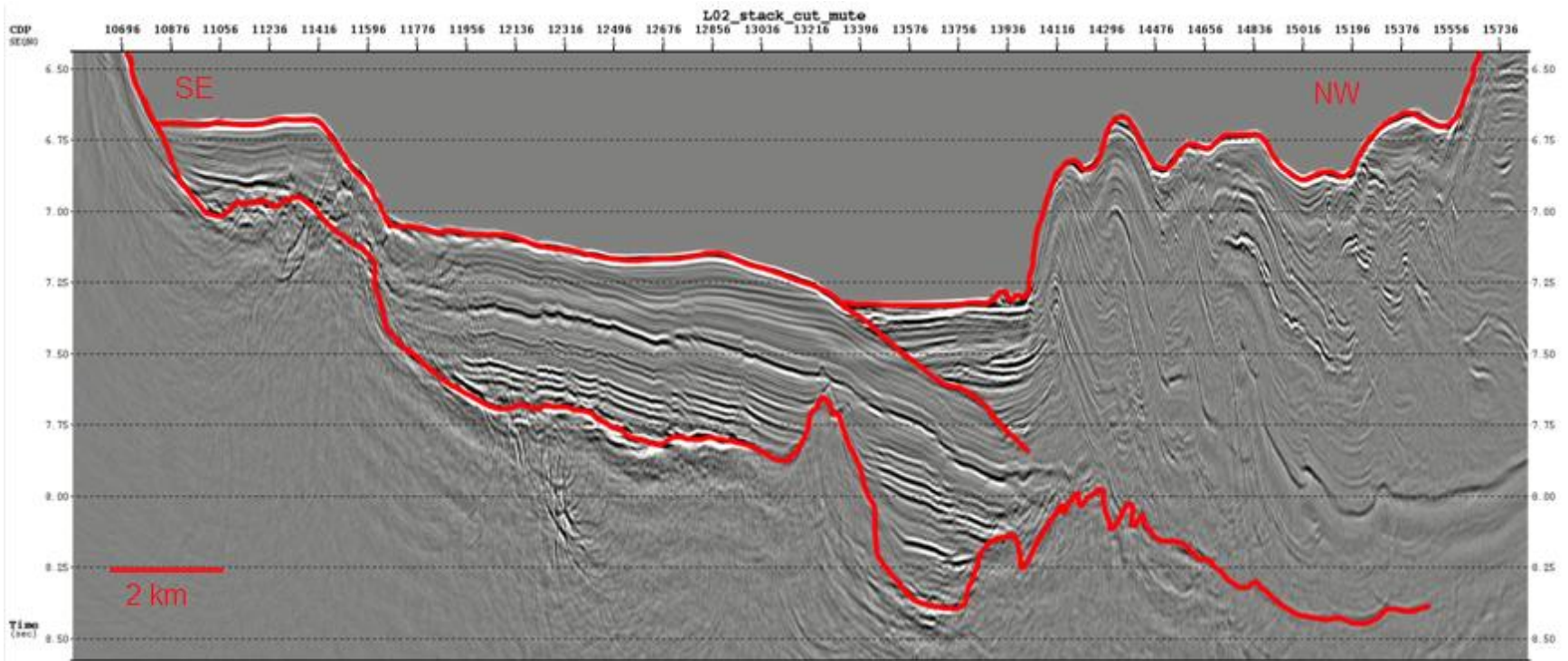


Figure 3.1.4b: Two distinct sediment packages are visible. The lower dipping down parallel the basement are the deep sea sediments accumulated since crust formation at ridge. The upper, horizontally layered trench sediments are likely terrigenous sediment sourced from the continent (Aleutian island chain).

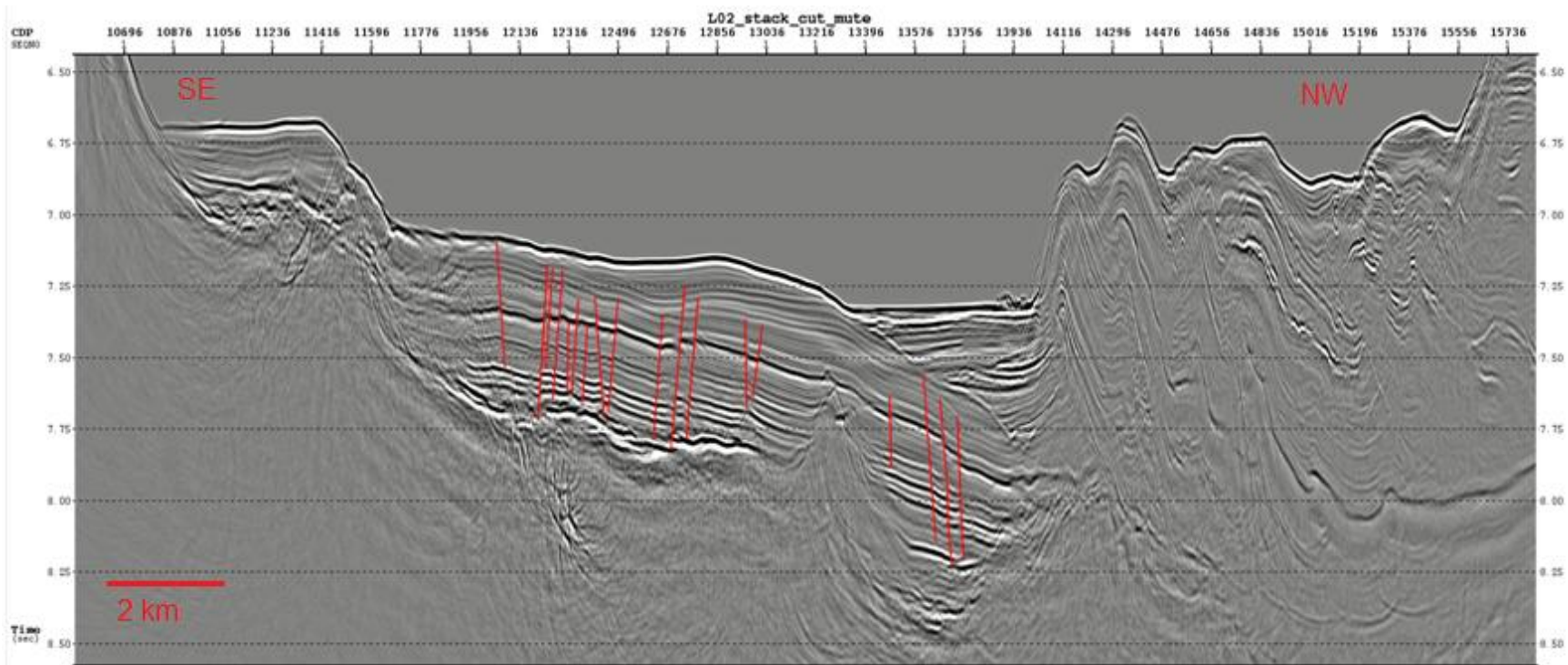


Figure 3.1.4c: Faulting is clear in the sediment and possibly upper crust. Faults are only present in the lower to middle sediment. Newer overlying sediment is undeformed.

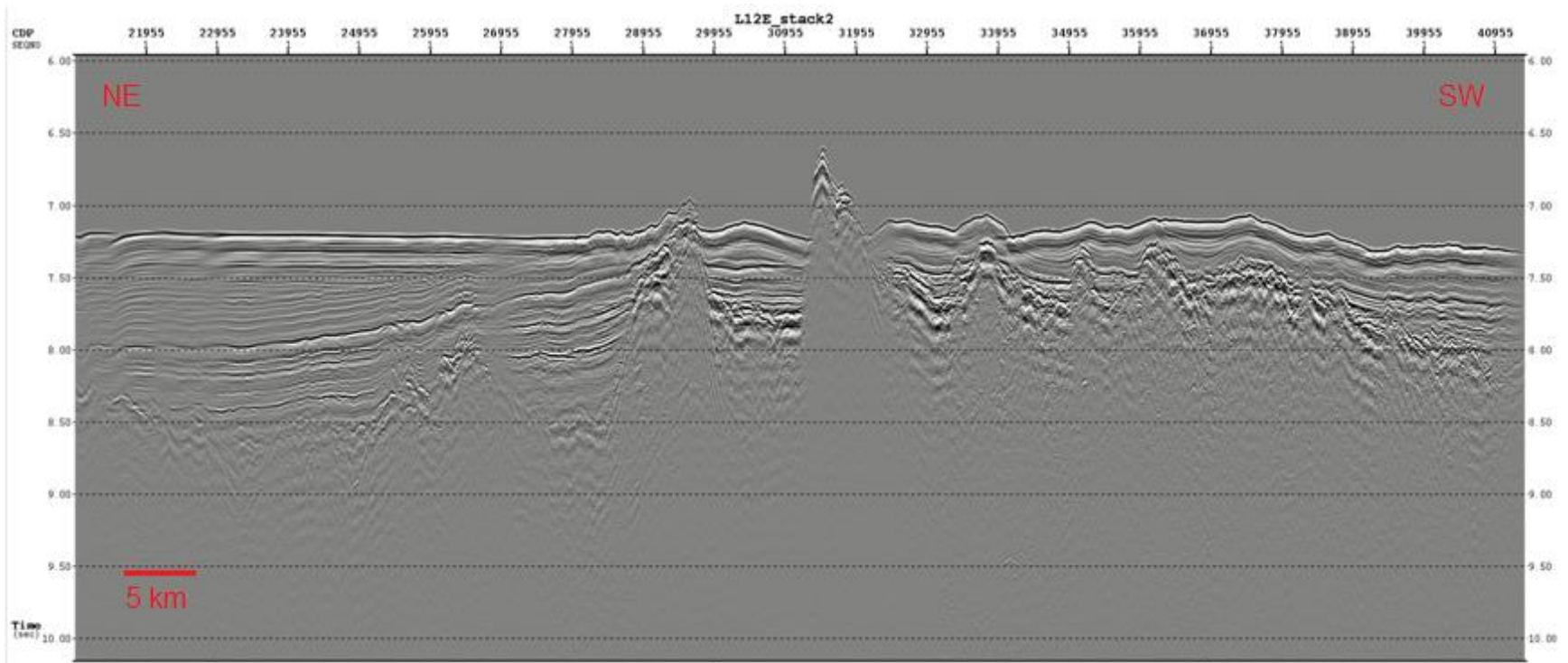


Figure 3.2.1: Full view of line 12E. Line was shot from northeast (left) to southwest (right). Basement topography appears very uneven and rough. There is a large lateral change in sediment thickness.

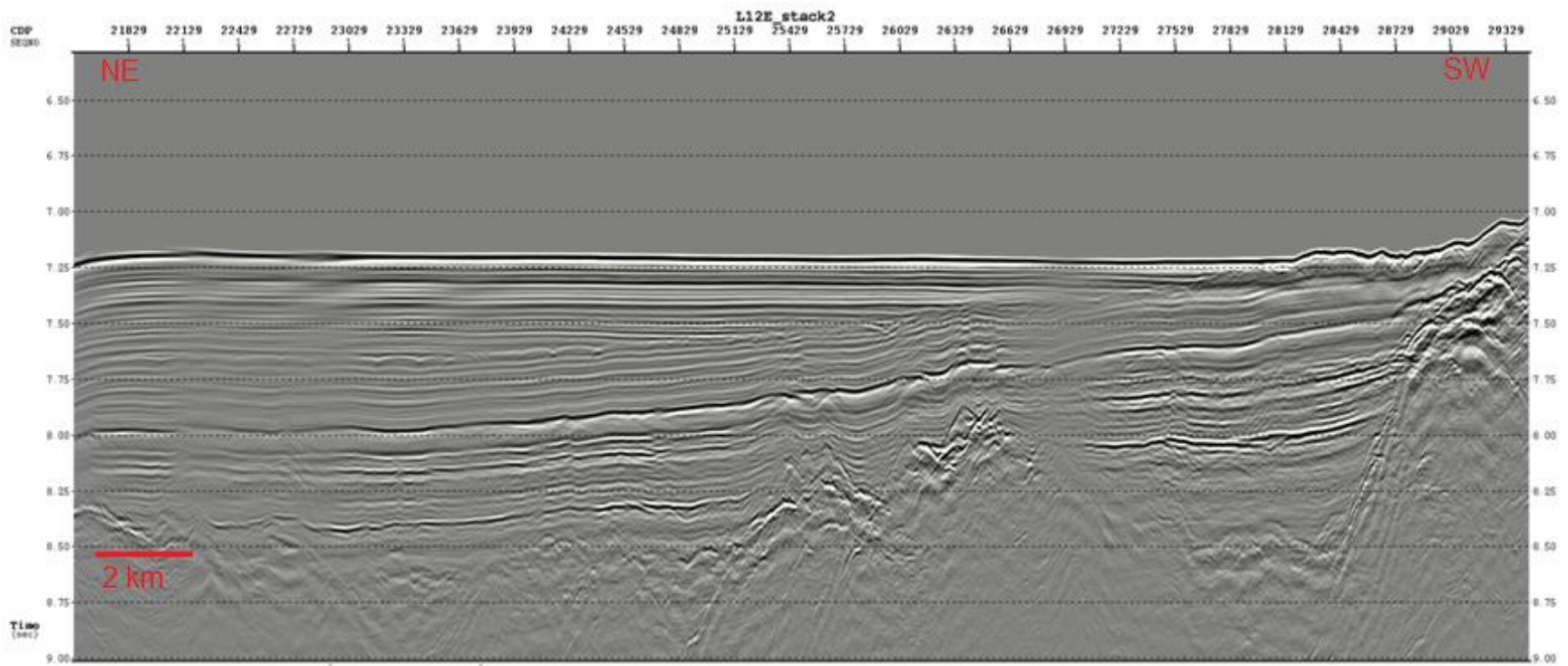


Figure 3.2.2a: Eastern side of line 12E. Sediment on the eastern side is much thicker than on the western portion of the line.

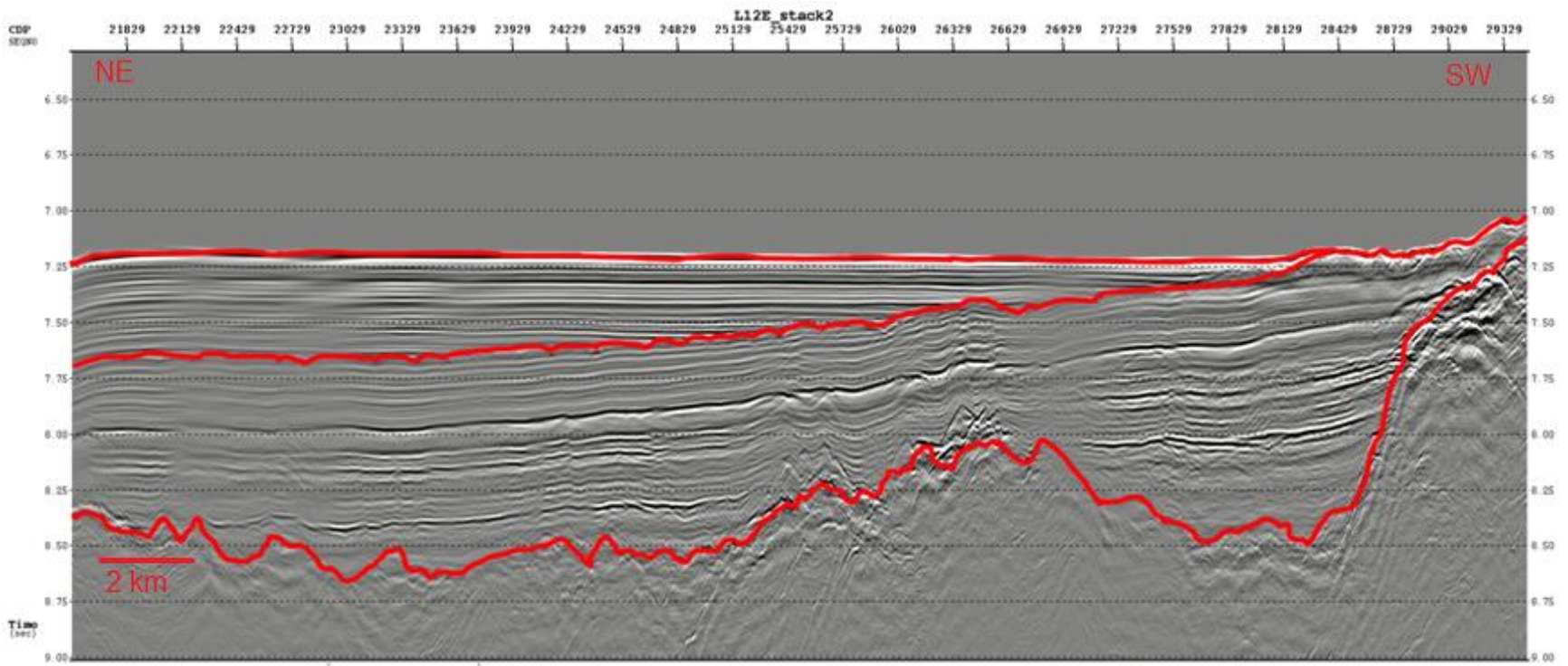


Figure 3.2.2b: Eastern side of line 12E. Two distinct cross cutting sediment packages can be observed.

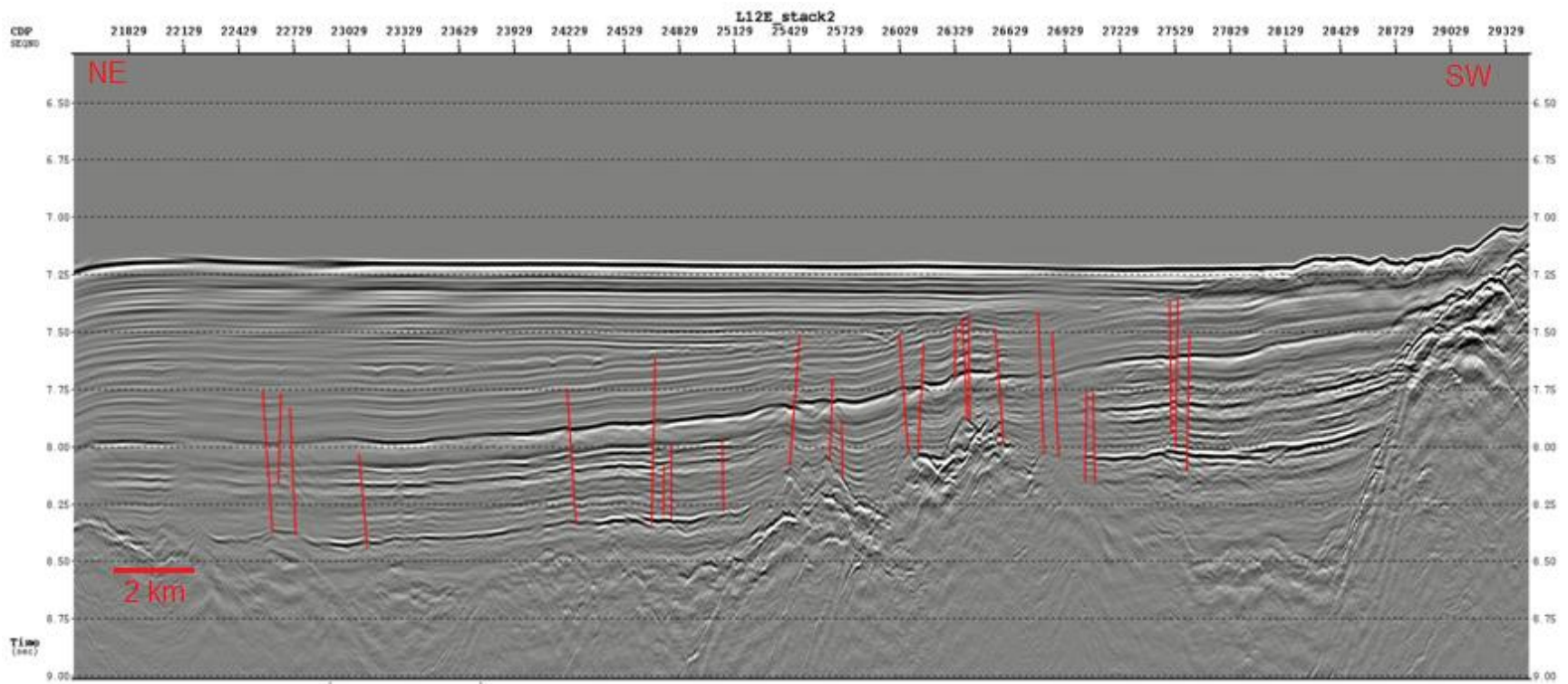


Figure 3.2.2c: Eastern side of line 12E. Small offsets can be seen in the pelagic lower sediment layers.

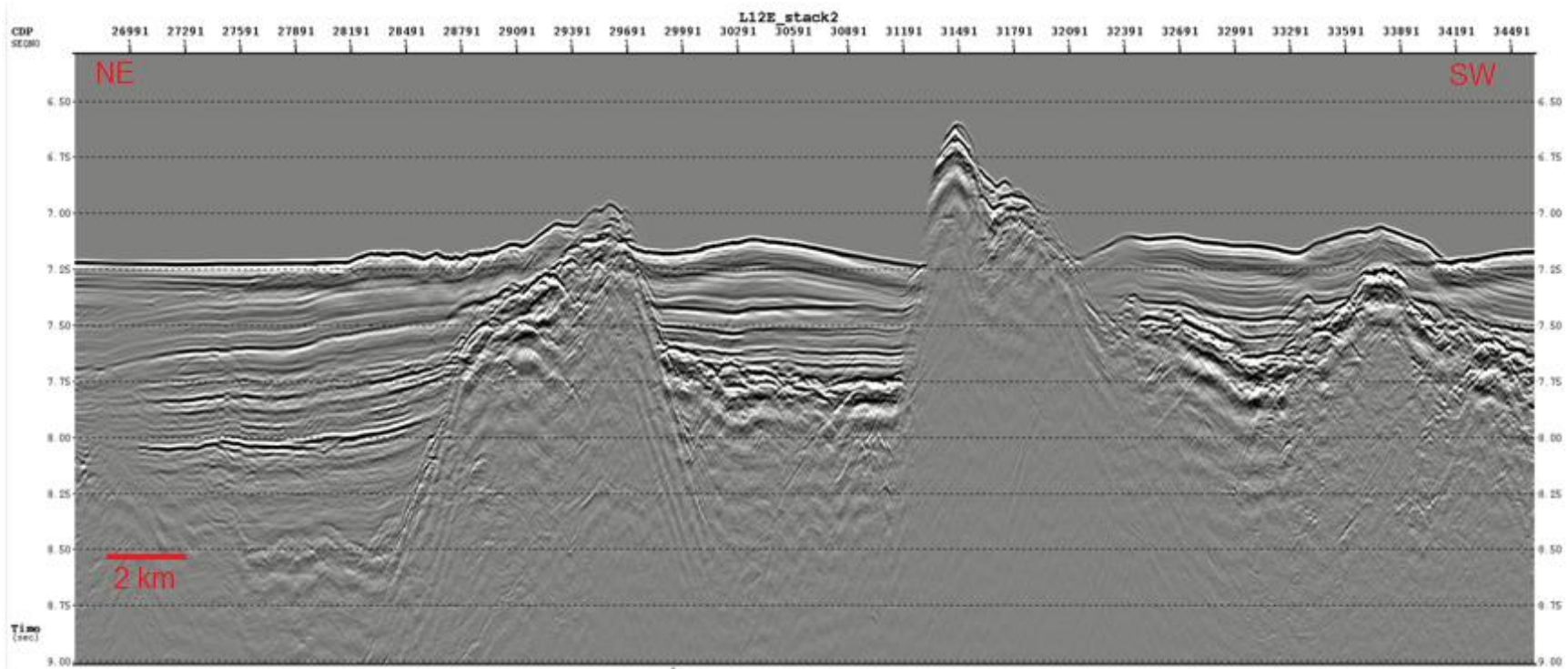


Figure 3.2.3: Center of line 12E (where it perpendicularly crosses line 2). Two distinct uprisings of basement occur where they appear to outcrop above the sediment.

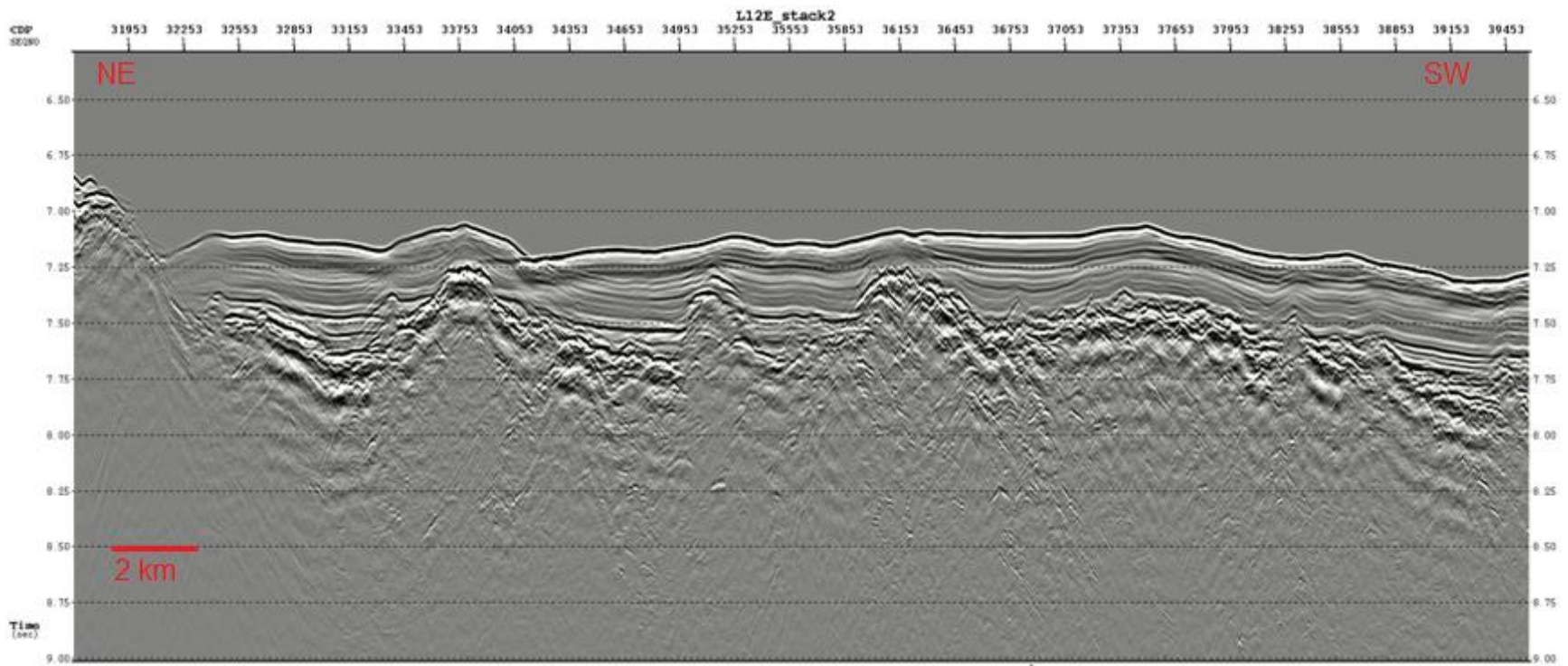


Figure 3.2.4: Western section of line 12E. Sediment cover is very thin relative to eastern side, with sediment cover following the rough basement profile.

#### 4. DISCUSSION

The most prominent structures imaged on 2 and 12E (Figures 3.1.1 and 3.2.1) are the seamounts, varying in height from 0.5 km to 1 km above the sediment laden seafloor. However, due to their distance from the trench, these structures will not have any effect on seismicity in the region for thousands of years. Along the Aleutian margin the Pacific plate is being subducted at an approximate rate of 63 mm/r (Sella et al., 2002). At this rate the seamounts seen on line 12E will not begin to subduct for another 87 thousand years, while the two seamounts on line 2 will not begin to subduct for approximately 349 thousand years and 873 thousand years respectively. Looking forward to when the seamounts do begin to subduct, we can first expect deformation of the upper plate's weak frontal prism, creating deep furrows where the seamounts erode the frontal prism (Kopp, 2013). The thick sediment cover in this region of the trench is likely sufficient to restore the prism once the seamounts have migrated through. Once subducted, these seamounts will also disrupt the planar surface of the megathrust, forming asperities.

Comparing processed line 2 with adjacent seismic lines in Shillington et al. (2014), there is a significant change along strike in the degree of faulting and sedimentation observed on the subducting plate (Figure 4.1.1 and 3.1.1). Imaged sediments are thinner in the Shumagin Gap, with accumulated sediments approximately half a kilometer thick, than in the Semidi segment further to the east which has approximately 600 m to 1 km of accumulated sediment being transported into the trench. Focusing on the Semidi segment (lines 2 and 4 on either edge, and line 3 crossing the centre) we see the sediment thickness is greatest in the centre of the segment, thinning out laterally to either end of the segment.

Large variations in the degree of faulting are observed over a relatively small area along the Alaskan trench, across the Shumagin Gap and the Semidi segment. On lines 5 and 6, imaging

across the Shumagin Gap, fault offsets reach a maximum displacement of 250 meters, spaced at approximately 2 to 5 km, producing a horst and graben structure. This in contrast to the faults imaged across the Semidi segment on lines 2 to 4 where the faulting is much less severe. Here faults have maximum fault offsets of 30 m, and fault spacing from 0.5 to 3 km. As discussed by Shillington et al. (2014), the bending faults observed in the Shumagin Gap are probably reactivated faults in the pre-existing ridge fabric because they lay within 10-25 degrees of the trench orientation. This is unlike at the Semidi segment where pre-existing ridge fabric is oriented approximately 70 degrees to the trench and new faults related to plate bending due to subduction are formed (Figure 4.1.2).

The gravity anomaly map for the study area (Figure 3.0.1a and 3.0.1b) indicates that the degree of plate bending at the outer rise is greater in Shumagin Gap than at the Semidi segment (where high anomaly values appear to be related to plate structures rather than bending at the outer rise). The relief of the outer rise continues to decrease eastward to mainland Alaska at the eastern extent of the Alaskan Trench. The decrease in plate flexure to the east could possibly be due to the interaction of the eastern margin of the subducting Pacific Plate with the North American Plate running perpendicular to the subduction zone. It is possible this trend in increasing amount of plate flexure moving westward could be a contributing factor to why we see less significant bending faults in the Semidi segment than in the Shumagin Gap further west.

Correlations can be made between the variation in plate characteristics along the margin, and the seismic activity seen along the margin. Referring to Figure 4.1.3 we see the Shumagin Gap is characterized by an abundance of both shallower (inter-plate) and deeper (intra-plate) earthquakes whereas both inter-plate and intra-plate earthquakes occur much more sparsely throughout the Semidi segment. A theory proposed by Ruff (1985) suggested that seafloors with

horst and graben structures will develop a heterogeneous contact plane with the overlying plate when subducted that will reduce the strength of mechanical coupling, whereas seafloors with thick sediments at the subduction zone will form a uniform plate contact plane with strong coupling. This proposal explains the variability in inter-plate seismicity between the Shumagin Gap and Semidi segment; the horst and graben structure subducting under the Shumagin Gap resulting in lower mechanical coupling and abundant earthquakes during the stick-slip process, while the abundant sediment subducting at the Semidi segment produces a large asperity surface with enhanced coupling, accounting for the lack of inter-plate seismicity in this area.

The intra-plate earthquake distribution appears to be tied to the degree of faulting at the outer rise; Higher instances of intra-plate earthquakes seem to occur in the Shumagin Gap where the extent of bending faulting is much greater than that of the Semidi segment. Kirby et al. (1996) proposed that intermediate depth earthquakes are triggered by dehydration reactions acting on the hydrous minerals in the subducting lithosphere, indicating that the distribution and frequency of intra-plate earthquakes is strongly influenced by the degree to which the lithosphere has been hydrated, with larger amounts of hydration resulting in larger occurrence of intra-plate earthquakes. Hydration of the crust is facilitated by faulting at the outer rise which implies the extent of bending faulting should be related to both the degree of lithospheric hydration and the quantity of intra-plate earthquakes observed. Shillington et al. (2014) showed, using P-wave velocity models based on wide angle seismic data, that the total hydration in the lithosphere was higher in the more extensively faulted Shumagin Gap than in the Semidi segment. This provides solid evidence for correlation between intra-plate earthquake distributions and bending faulting at the outer rise.

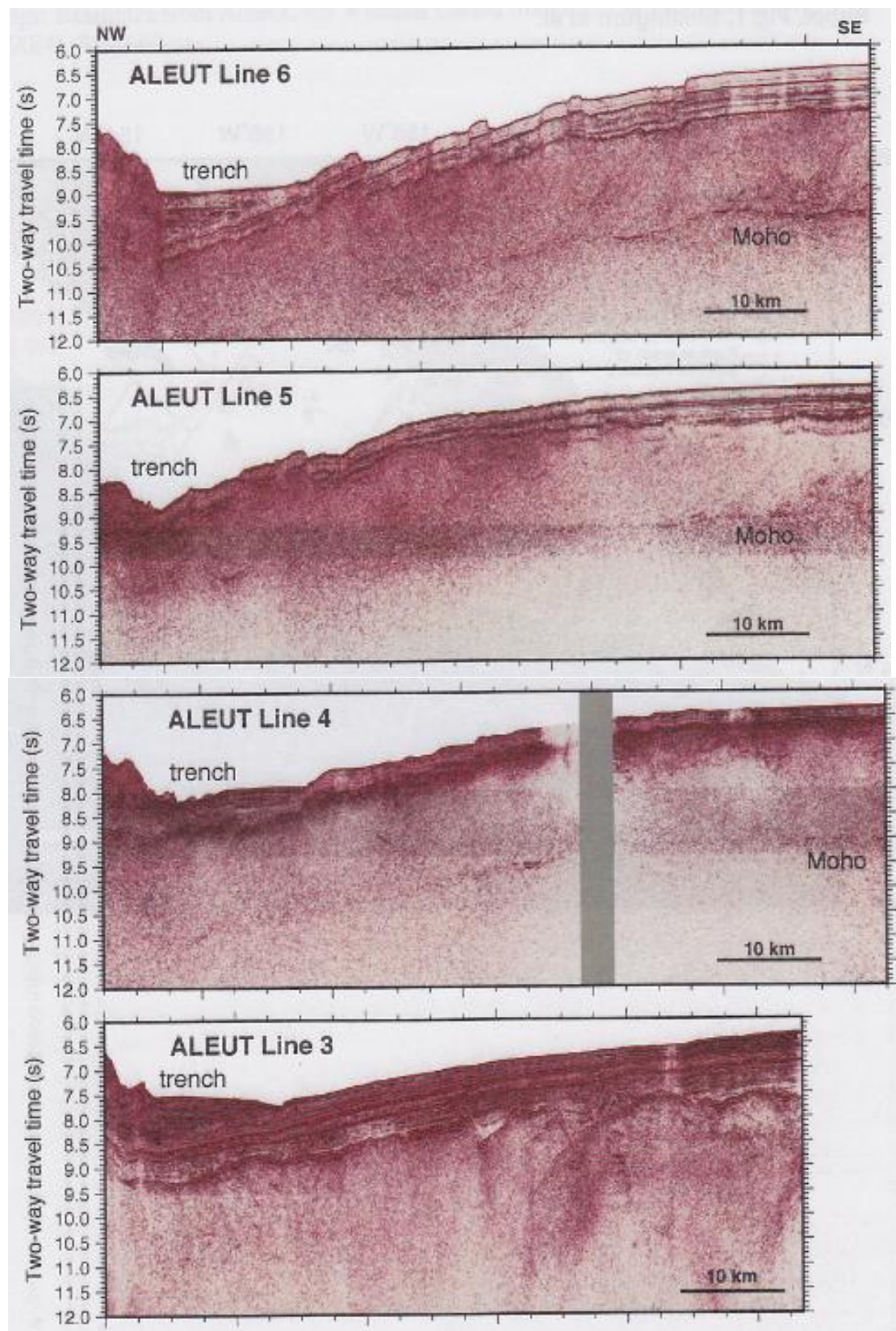


Figure 4.1.1: Lines 3, 4, 5, 6 all running perpendicular to the trench. Lessening degrees of bending faulting are evident moving from line 6 in the Shumigan Gap to line 3 in the Semidi segment (After Shillington et al., 2014).

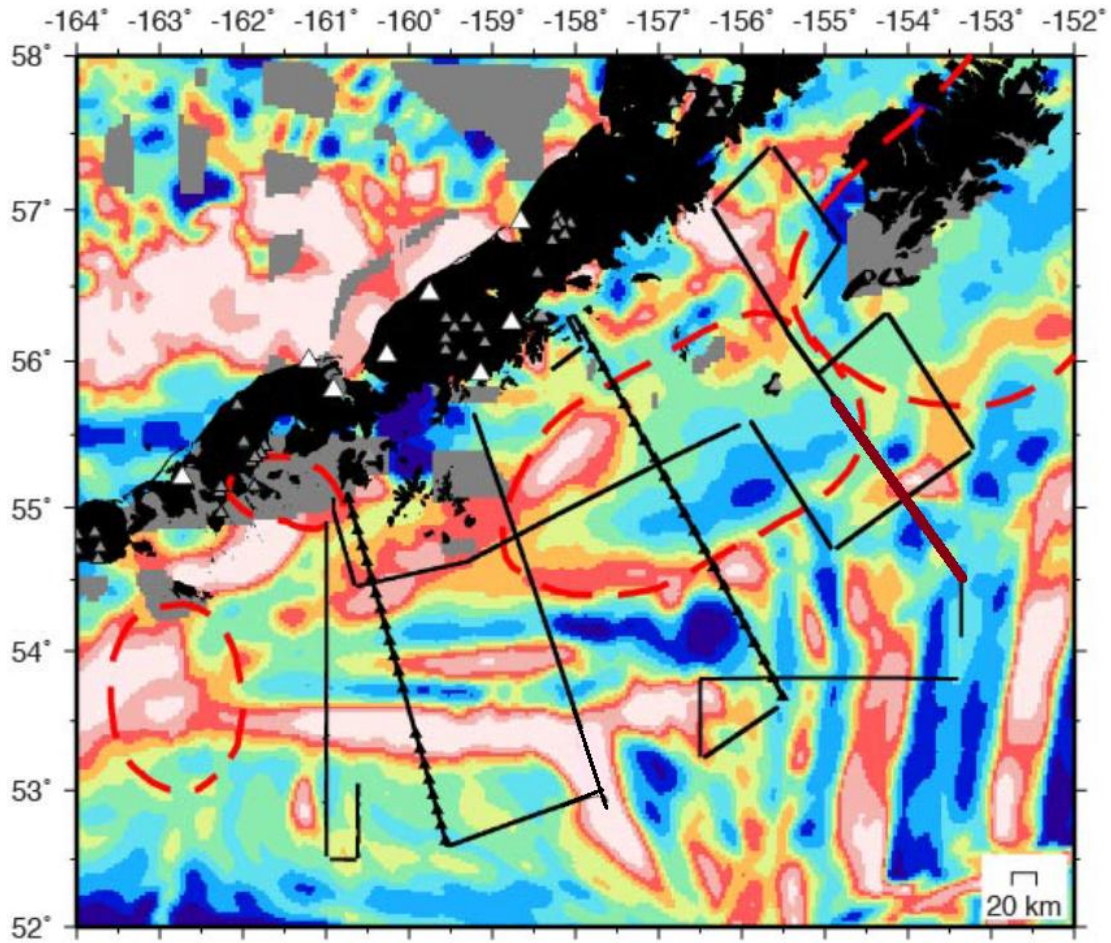


Figure 4.1.2: Magnetic anomaly map displaying orientation of ocean crust fabric. Processed section of Line 2 is highlighted in dark red. Note the high angle between the subducting crust fabric at line 2 and northeast southwest trending Alaskan trench (After Shillington et al., 2014).

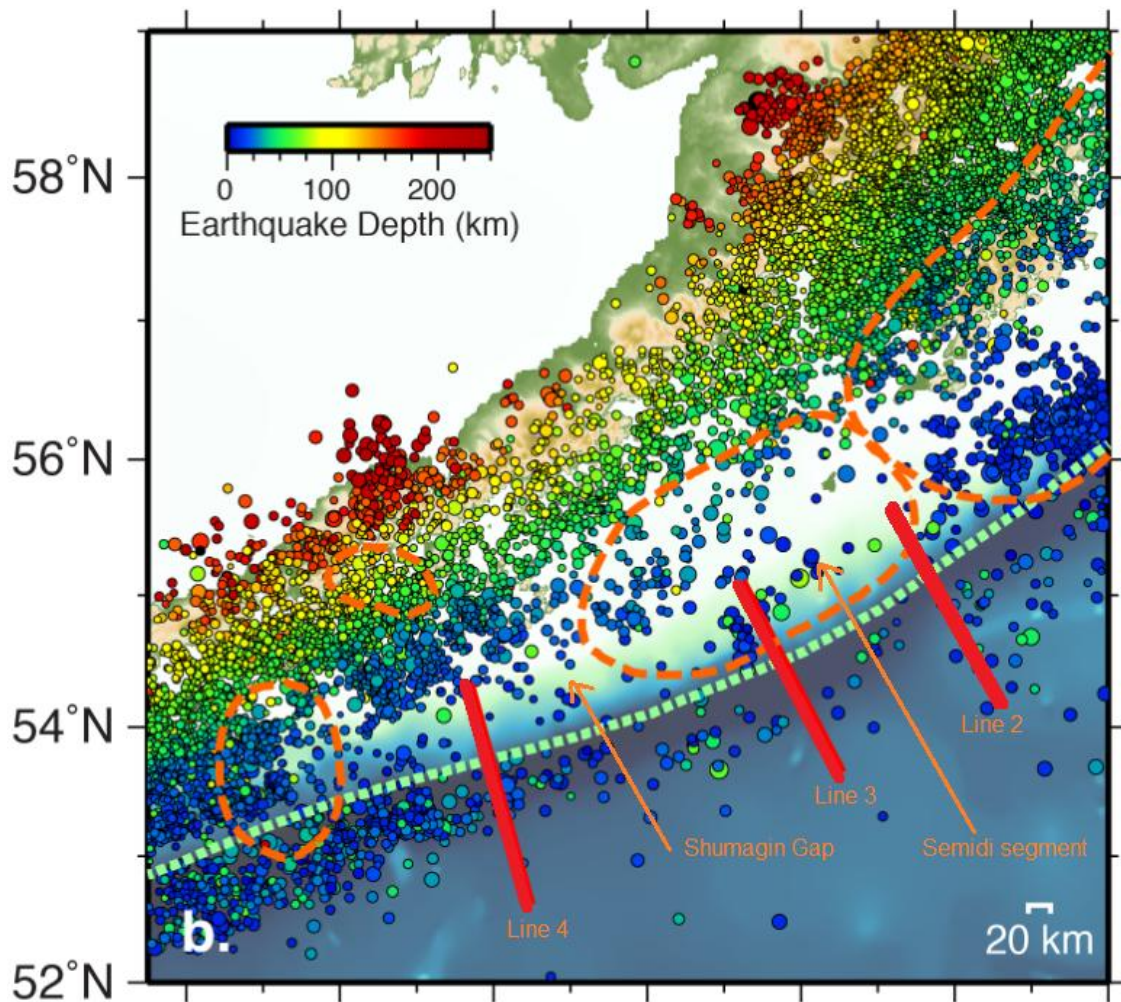


Figure 4.1.3: Distribution of earthquakes along the section of the Alaskan subduction zone examined in study (After Shillington et al., 2014)

## LITERATURE CITED

Kirby, S. H., E. R. Engdahl, and R. Delinger (1996). Intraslab earthquakes and arc volcanism: Dual physical expressions of crustal and uppermost mantle metamorphism in subducting slabs, in *Subduction: Top to Bottom*, Geophys. Monogr. Ser., vol. 96, edited by G. E. Bebout et al., pp. 195-214, AGU, Washington, D. C.

Kopp, H. (2013). Invited review paper: The control of subduction zone structural complexity and geometry on margin segmentation and seismicity. *Tectonophysics*, 589, 1-16.

Ruff, L. J., 1989. "Do trench sediments affect great earthquake occurrence in subduction zones. *Pure and Applied Geophysics* 129, 263-282.

Shillington, D. J., Becel, A., Nedimovic, M. R., Kuehn, H., Webb, S. C., Abers, G. A., et al. (2014). Controls on abrupt changes in faulting, hydration and seismicity in the Alaska subduction zone. 1-19.

Yilmaz, O., & Doherty, S. M. (2001). *Seismic data analysis: processing, inversion, and interpretation of seismic data* (2nd ed.). Tulsa, OK: Society of Exploration Geophysicists.